CO2 Human Emissions

LES Simulation Report

A Klonecki

P. Prunet

Co-ordinated by ECMWF

D2.8 LES simulation report

Dissemination Level:	Public
Author(s):	Andrzej Klonecki, Pascal Prunet (SPASCIA)
Date:	28/19/2020
Version:	1.0
Contractual Delivery Date:	04/06/2020
Work Package/ Task:	WP2/ T2.6
Document Owner:	SPASCIA
Contributors:	SPASCIA
Status:	Final

CHE: CO_2 Human Emissions Project

Coordination and Support Action (CSA)
H2020-EO-3-2017 Preparation for a European capacity to monitor CO_2 **anthropogenic emissions**

Project Coordinator: Dr Gianpaolo Balsamo (ECMWF)
Project Start Date: 01/10/2017
Project Duration: 39 months

Published by the CHE Consortium

Contact:
ECMWF, Shinfield Park, Reading, RG2 9AX,
gianpaolo.balsamo@ecmwf.int

The CHE project has received funding from the European Union's Horizon 2020 research and innovation programme under grant agreement No 776186.

Table of Contents

Figures

1 Executive Summary

Point sources, such as fossil fuel burning power plants, steel production plants and refineries are key emitters of CO_2. Because they can undergo large variations in emissions over time due to, for example, changing economic conditions, the monitoring of their emissions, especially in the context of recent climate treaties, is important. Europe, in particular, is developing a system to support Monitoring, Reporting and Verification (MRV) of various CO_2 sources based on a combination of space-borne and ground-based measurements.

CO_2 flux inversion approaches that rely on space data are currently, and also in the near future, based on low-orbit polar satellite instruments that provide only episodic sampling of CO_2 plumes. These snapshots correspond only to a representation of transport during the overpass of the satellite. Under turbulent conditions, the plumes show a strong temporal variability and their shape differs from the generally assumed Gaussian plume shape.

In this work we use the EULAG LES model to simulate the spatio-temporal variability of the CO_2 plume in the vicinity of strong sources. The realism of the model simulated transport is evaluated against measurement data from the CoMet campaign on 7 June 2018 over the Bełchatów power plant in central Poland. Next the impact of the LES simulated variability on two top-down flux retrieval methods is analysed. For the Optimal Estimation Method (OEM), we provide a preliminary quantification of the relative model error due to its inherent inability to reproduce the stochastic features of turbulent transport. For the Mass Balance method, we analyse the impact of the non-Gaussian shape and of the presence of pockets (or puffs) with high CO_2, on the individual line densities at various distances from the source. Given the high variability in our line density estimates, while depending on the swath width and the part of the plume being imaged, the mean flux values retrieved from a simple overpass will be affected.

The work presented in this report is issued from work in progress. The perspectives are provided in a dedicated section.

2 Introduction

2.1 Background

Anthropogenic emissions of CO_2, mostly from burning of fossil fuels, have led to a pronounced increase of CO_2 concentrations in the Earth's atmosphere. It is widely accepted that this increase has been the main driver behind the raising of global temperatures at the Earth's surface observed over the last several decades.

Scientists, policy makers, governments and the civil society in general have recognised the risks linked to anthropogenic emissions of CO_2 and other greenhouse gases and have taken steps to limit their emissions. In particular, at the Paris 2015 United Nations **Climate Change Conference**, COP 21 (Conference of Parties), the so-called Paris Agreement was negotiated. All participating countries must every five years report to the UNFCCC secretariat the national contributions (NDC = Nationally Determined Contributions) that summarize their efforts to reduce their emissions. The currently reported emissions are based on socio-economical data, like the number of cars or the electricity production from power plants. Independent verification by comparison with emission estimates based on observations of atmospheric greenhouse gases is largely absent, yet much needed. Hence, it is important to provide such support an verification means. Europe, in particular, is developing a system to support Monitoring, Reporting and Verification (MRV) of CO_2 emissions for climate agreements based on a combination of space-borne and ground-based measurements. The current CO_2 Human

Emissions (CHE) project is a major effort that explores the development of such a system at various spatial scales including emissions from cities and local point sources.

Point sources, such as fossil fuel burning power plants, steel production plants and refineries are key emitters of CO_2. Because they can undergo large variations in emissions over time due to, for example, changing economic conditions, the monitoring of their emissions at the facility level is important (Ciais *et al*.,2015 , Nassar *et al*., 2017). Precursor studies on the estimation of CO_2 emissions from strong point sources based on space-based measurements have been recently published based on e.g. GOSAT-2 and OCO-2 data (Nassar *et al*., 2017). These approaches rely currently on low Earth orbit (LEO) polar instruments that provide only episodic, narrow-swath snapshot views of the plumes emitted from these sources. GOSAT has non-contiguous FOVs of 10.5 km (large distances between soundings) with a revisit time of 3 days while OCO-2 has a swath of 10km (8 pixels in across track direction) leading to a revisit time of 16 days (see Figure 1 for illustration of viewing geometries). Future imaging instruments will provide a wider swath that will capture the extent of the plume cering several tens of kilometres but will still be subject to limited temporal sampling for the short time of the overpass. The presence of clouds and possible perturbing effects of aerosols will limit the number of exploitable observations available in a single year. The impact of cloud coverage on the number of detected power plant CO_2 plumes from CO2M was estimated recently by Kuhlmann *et al*., 2019. For a constellation of 6 CO2M satellites with 250 km swath each and 2x2km FOV, plumes from a strong emission power plant (Jänschwalde) could be observed on about 40–45 days per year.

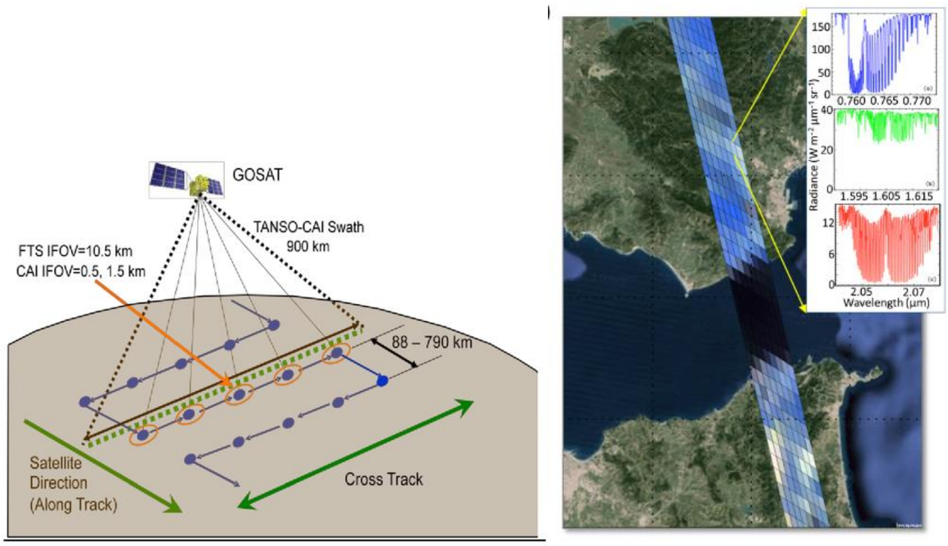

Figure 1:Observation geometries for left: GOSAT (figure from Hamazaki et al., 2017) and right: OCO-2 (figure from Crisp et al., 2016).

The snapshot nature of observations will have two major impacts:

1) The observations will only lead to estimates of emissions at the time of overpasses or shortly before it (the fossil fuel power plant stations do not function at their full capacity at all times)
2) The measured plume strength (XCO_2 = column averaged dry air CO_2 mixing ratio) and plume pattern correspond to a given realisation of transport from the source to the measured pixel. Under turbulent conditions, the resulting plume can be characterized by strong spatio-temporal variability that will result in a non-Gaussian, non-continuous plume. Such nature of the plume will possibly have a strong impact on the results of any flux inversion studies for point sources based on currently used top-down methods

such as: a) analytical inversions in which model simulated values are matched against observations using e.g. optimal estimation method and b) mass-balance approaches in which the estimated flux, based on the measured column and information on plume speed and direction, is integrated along a surface perpendicular to the plume main longitudinal axis.

It is the impact of the spatio-temporal variability of plume pattern and strength (second of the two impacts listed above) that is examined in this report. In the analytical method using incorrect position and shape of the puffs that transport CO_2 under turbulent transport conditions can lead to erroneous flux estimations. Given the random nature of turbulent transport, transport model uncertainties need to be considered as an additional uncertainty term in these inversion studies. Flux inversions based on the optimal estimation approach allow considering the various uncertainty terms to weigh the observational and *a priori* knowledge terms during the minimisation of the cost function. In the mass balance approach, the presence of multiple XCO_2 maxima in a given plume (puffs) will also lead to a potentially wide range of flux estimations depending on the distance from the source and the part of the plume that is sampled by observations.

In this study we propose a first attempt to characterize the spatio-temporal variability of transport processes for local scale plumes from power plants. The approach used is based on simulations performed with a high spatial resolution Large Eddy Scale model (LES), the analysis of the LES simulated spatio-temporal variabilities, and the comparison with measurements and simulations from other models. The study is performed for a particular meteorological situation during the CoMet measurement campaign on June 7, 2018 in the vicinity of the Bełchatów power plant in Poland. The objective is to demonstrate the pertinence and interest of the approach, and to derive an objective method from this case study to generalise and consolidate the estimate of the uncertainty from transport processes at local scale and further use this uncertainty in flux inversion methods.

2.2 Scope of this deliverable

2.2.1 Objectives of this deliverables

Task 2.6: Perform very high-resolution (~100 m) LES simulations of the spatio-temporal variability of CO_2 in a power plant emission plume using realistic meteorological input from Task 2.3 to represent plume dispersion in different meteorological regimes. Perform focused comparisons with high resolution regional simulations of Task 2.3 and analyse potential differences at the typical scale of measurements from an imaging satellite. Using the LES simulations and an orbit simulator, test whether the CO_2 emissions can be recovered from the XCO_2 measurements of an imaging satellite, e.g. by matching a Gaussian plume model.. Recommendations for the characterisation of the so-called representation errors, due to the small scale and fluctuating nature of power plant plumes not represented in emission retrieval schemes, will be provided.

2.2.2 Work performed in this deliverable

In this deliverable we present the results of the work on the modelling of CO_2 plume transport from strong point sources (power plants) using the LES EULAG model. The model was adapted to take as driving meteorological fields the output from the mesoscale COSMO-GHG model (Task 2.3). The LES results were compared against measurements from the CoMet campaign on 7 June 2018 in order to judge the realism of the simulations. Next, the spatio-temporal variability in the LES results was analysed. We preliminarily quantify this variability in order to provide a preliminary estimate of the direct model uncertainty due to the stochastic dynamics of the plume under highly turbulent conditions. Next, we look at the impact of spatio-temporal variability on the mass balance CO_2 flux retrieval method.

2.2.3 Deviations and counter measures

There were no deviations.

3 Description of EULAG model setup

3.1 Brief description of EULAG model

EULAG is NCAR's generic numerical framework for solving geophysical flow equations for a wide range of scales and applications. It allows solving the equations of fluid motion in either the EULerian or the semi-LAGrangian mode (Prusa *et al*., 2008). The code has been used, in particular, to simulate turbulent flows in the large-eddy simulation mode (LES), in which the large scales of turbulence are explicitly resolved on the model grid and the remaining sub-grid scales are parameterised.

EULAG is a research code that allows multiple adaptations based on particular user needs. The LES EULAG version used in this project solves the anelastic Navier-Stokes equations in the Eulerian form (Wyszogrodzki *et al*., 2012).

3.2 Work performed on the EULAG model in the framework of the CHE project

Several specific model adaptations of the EULAG version described in Wyszogrodzki *et al*., 2012 were performed in this project. In particular, the model was coupled with the Task 2.3 output from the mesoscale model COSMO-GHG. The following meteorological output fields from COSMO-GHG were used to initialize the EULAG simulation as well as to force the model throughout the simulation:

- 3D u, v and w wind velocity fields
- 3D temperature profile
- 3D pressure profile
- 3D humidity profile
- surface sensible heat flux

The COSMO-GHG fields provided at 1-hour resolution and on a 1 km ×1 km grid were interpolated to EULAG spatial grid and time steps.

In the current LES simulations, the surface topography is also taken from the COSMO-GHG model (at 1 km ×1 km). Increasing the resolution of topography to correspond to the resolution of the LES model is one of the possible improvements.

The EULAG model was set up for a domain including the Bełchatów power plant in central Poland. The model was modified to run with two passive tracers corresponding to emissions of CO_2 from the two 320 m high emission stacks of the power plant.

A different mode for running the code consisted of driving the model not with mesoscale meteorology but with a constant-in-time set of atmospheric parameters derived from aircraft CoMet *in situ* measurements. The surface sensible heat flux, that has a strong impact on the onset of turbulence, was in this case fixed to a representative number and sensitivity studies were performed to test its impact. The results described in this report correspond only to the time varying forcing based on the COSMO-GHG model.

3.3 EULAG model setup used for the CHE project

Various configurations of the EULAG model were tested. The results shown in this report were obtained for a domain of 320 grid points in the longitudinal and 256 in the latitudinal direction. The size of a single grid cell corresponding to the model spatial resolution is 200 m. The projection used follows the latitude-longitude lines. The total domain covers a region of 64 km × 51.2 km over central Poland and contains most of the CoMet measurements. The locations of the two Bełchatów stacks are indicated with crosses in Figure 2. The dominant wind in the boundary layer being from east and south east, the power plant is placed sufficiently far from model boundaries to allow the build-up of high resolution up-wind circulation in the model domain.

The vertical resolution of the model grid is 40 m. With 60 model levels, the model thus extends to 2400 m above the surface (for the case studied here, this altitude is above the top of the boundary layer). The vertical coordinate is a surface-following one.

The temporal time step of the model is 0.5 s, with model output stored every 2 minutes. The total length of the simulation that allows to cover the duration of the CoMet flight is 300 minutes. With the T0 at 11 AM on 7 June 2018 (date of the CoMet flights), the first one-hour period is devoted to model initialisation and plume formation.

The two passive tracers correspond to the CO_2 emitted separately from the two power plant stacks, which are about 350 m apart. Only the CO_2 enhancement due to emissions from the stacks is simulated; the background CO_2 levels for comparison with observations is fixed at the measured value of 400 ppmv in the well mixed boundary layer.

The total strength of CO_2 emissions for Bełchatów was fixed at 38 MtonCO_2/yr (mega ton of CO_2 per year). An assumption is made that both stacks emit half of this amount. The emission height was prescribed based on plume rise results from a study performed by EMPA using the approach described in Brunner et al., 2019. Two values for the vertical position of the plume injection heights were tested: 620 m and 827 m above surface, which is considerably higher than the stack height of 320 m. The values used correspond to the effective plume rise altitude resulting from the original buoyancy of the emissions at the stack top and from the specific meteorological conditions on 7 June 2018. It is assumed that the CO_2 is released with a Gaussian vertical distribution with sigma = 240 m about the prescribed emission height. In the results presented in this report, it is assumed that during the vertical rise to the injection height, the plume gets horizontally diffused. For each stack, the CO_2 is thus emitted into 25 grids (5x5, or 1 km x1 km) centred on the model grid containing the stack. Emitting the CO_2 into a single horizontal model pixel resulted in highly concentrated CO_2 values leading to disagreement with observations.

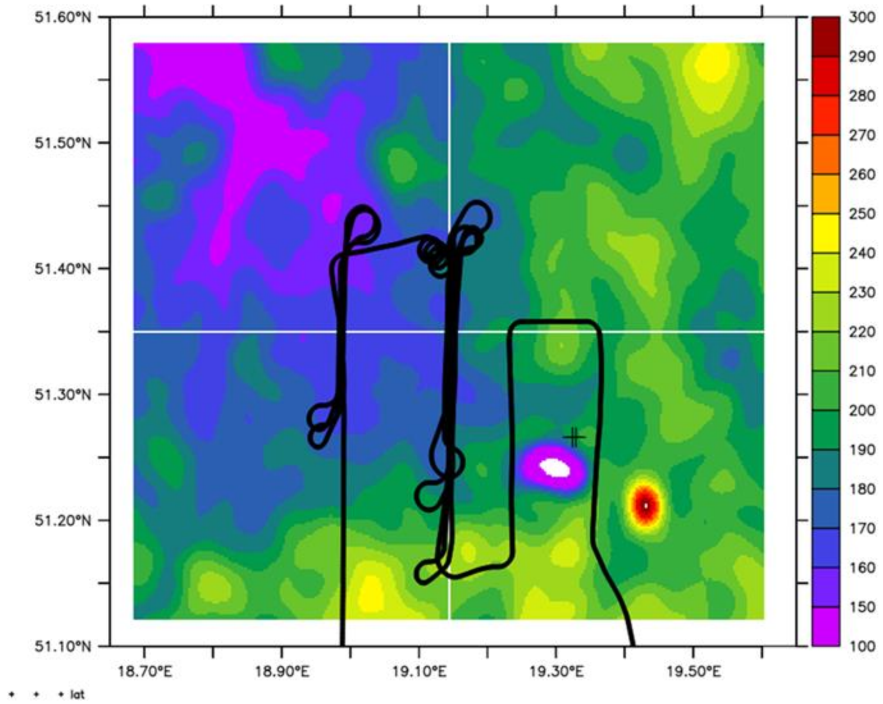

Figure 2: Spatial domain selected for the EULAG LES model. The colour scale indicates the topography used (interpolated from 1 km × 1 km COSMO-GHG output). The two '+' symbols (almost coinciding at the scale of the figure) indicate the positions of the two stacks of the Bełchatów power plant. The black curve indicates the portion of the flight path of the DLR aircraft on 07.06.2018 (during the CoMet campaign) that is contained within the EULAG domain. The EULAG model was run on four processors with each processor solving the equations for one of the spatial regions indicated in the figure.

4 Evaluation of EULAG simulations with CoMet data

4.1 Description of CoMet data

In order to validate the spatio-temporal variability simulated by the model and used in section 5 to estimate the resulting model variability, the model results are compared against measurements from the CoMet campaign from the flights around the Bełchatów power plant on 7 June 2018. Two types of measurements collected during CoMet were used in this project:

- *in situ* aircraft (D-FDLR) measurements from DLR (CO_2, CH_4, wind direction and speed, temperature)
- CO_2 total column enhancement from University of Bremen MAMAP airborne instrument flown on a different aircraft.

The DLR measurements were obtained during a single flight with measurements available from 13:30 UTC till 15:30 UTC. Figure 3 shows the flight path of the aircraft as a function of altitude, with the colour of the pixels indicating the time of measurements. The black line corresponds to the projection of flight path on the surface. The aircraft first flew upwind from the power plant (wind mostly from east and south-east in the boundary layer). Next it flew downwind of the stacks with several direct interceptions of the power plant plume. The changing altitude of the plane allowed to measure the CO_2 penetration into the upper part of the boundary layer. In the second part of the flight, the aircraft performed two altitude ascents from 750 m to the free troposphere: the first ascent at about 20 km and the second at about 35 km from the source. The MAMAP CO_2 column enhancement was measured during two overflights: first from 12:20 UTC till 13:27 UTC and second from 13:27 UTC till 14:45 UTC

(Figure 4). The column enhancements for each of the two overflights were obtained from 7 separate transects, with the location of the transects being very similar for the 2 overpasses

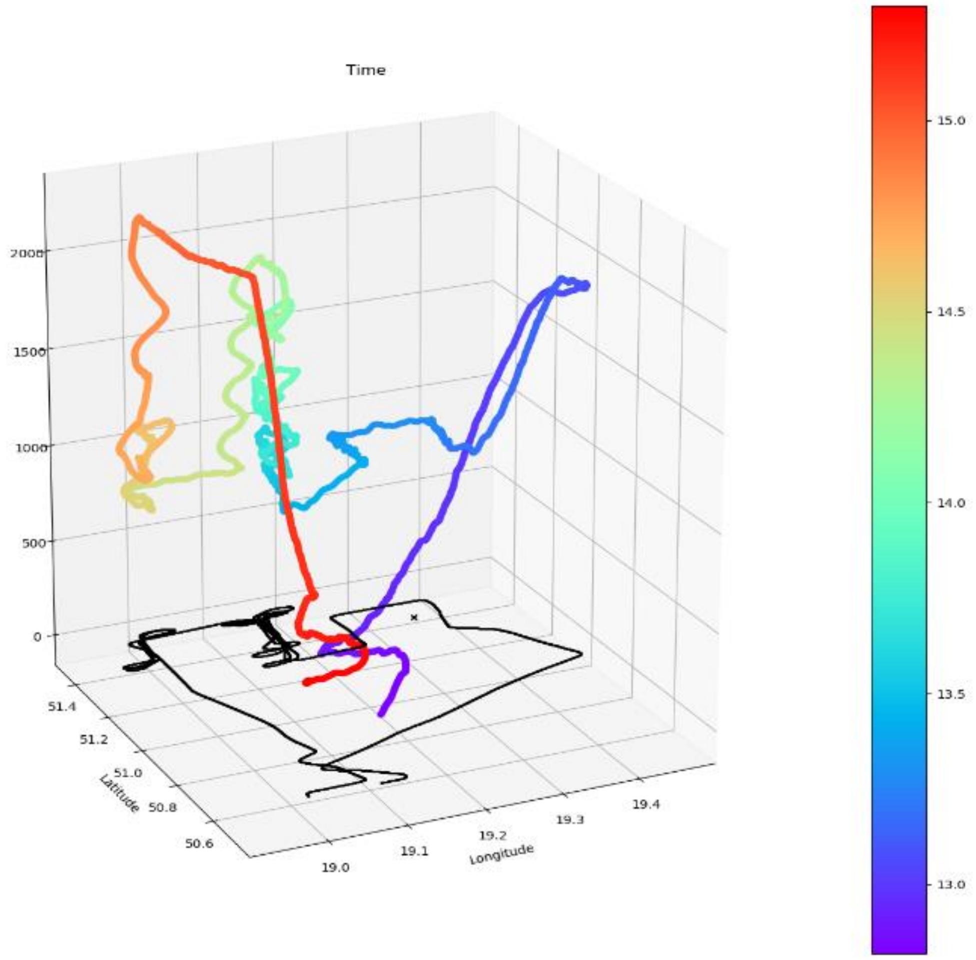

Figure 3: DLR aircraft flight path during CoMet flight on 07.06.2018. The colour scale indicates the time of the measurement. The black curve indicates the projection of the flight path on the ground. The small x symbols indicate the positions of the two Bełchatów stacks.

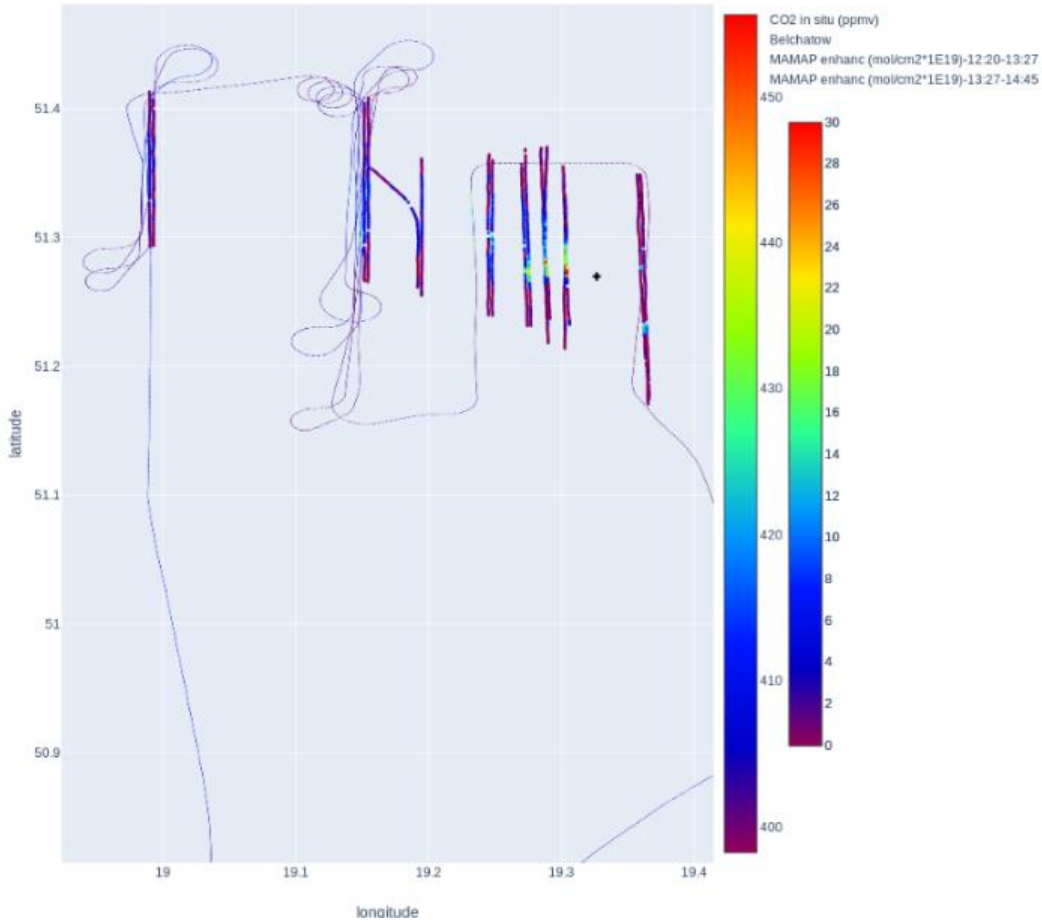

Figure 4: MAMAP CO_2 column enhancements from two CoMet flights on 07.06.2018. The colour scale indicates the column enhancement with respect to background in molecule/cm^2. The transects from the two flights were made on very similar positions.

The wind directions measured by DLR are indicated in Figure 5. In the boundary layer the wind direction was mostly from the south-east, while in the lower free troposphere, where CO_2 background was substantially higher, the wind direction changed by 180° being mostly from west and north-west.

Figure 6 indicates relatively strong variability in wind direction in the boundary layer with winds changing by ±50° around the mean as well as presence of vertical wind shear. The wind shear is particularly strong between 1500 m and 2000 m, that is in the transition zone between the well mixed boundary layer and the free troposphere. No major changes in wind direction between the start and end of the measurements were observed. The wind speed (Figure 7) varied between 0 and 8 m/s with mean values of about 5 m/s in the boundary layer. The horizontal wind is generally weaker in the free troposphere.

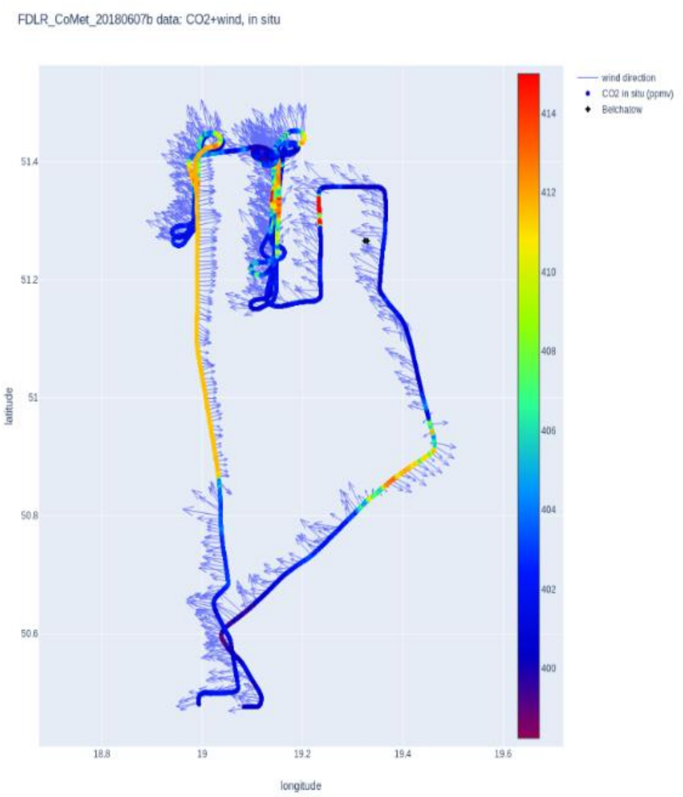

Figure 5: The arrows indicate the *in situ* horizontal wind direction from DLR measurements (CoMet flight on 07.06.2018). The colour scale indicates corresponding measured *in situ* CO_2 values (ppmv). The small x symbols indicate the positions of the two Bełchatów stacks.

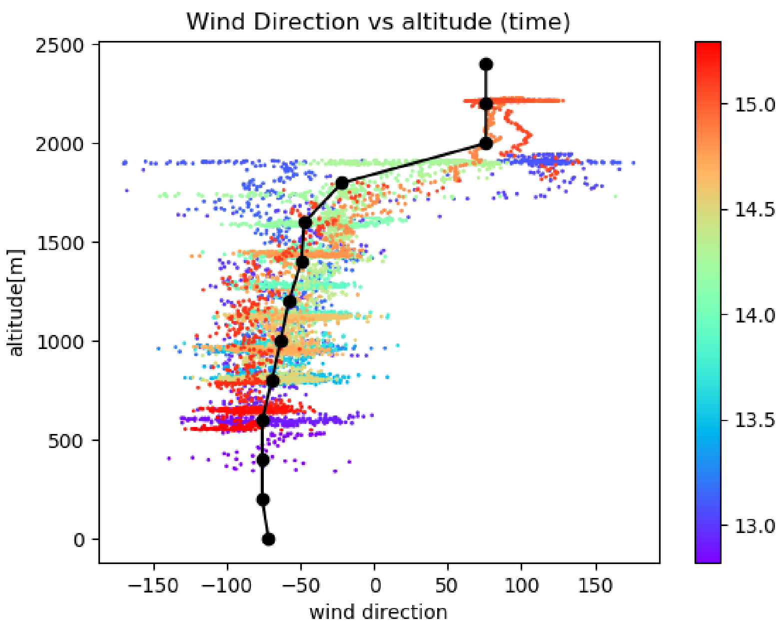

Figure 6: The *in situ* wind direction from DLR measurements (CoMet flight on 07.06.2018) plotted as a function of altitude above sea level. The colour scale indicates the time of the measurement. The black dots indicate the mean profile.

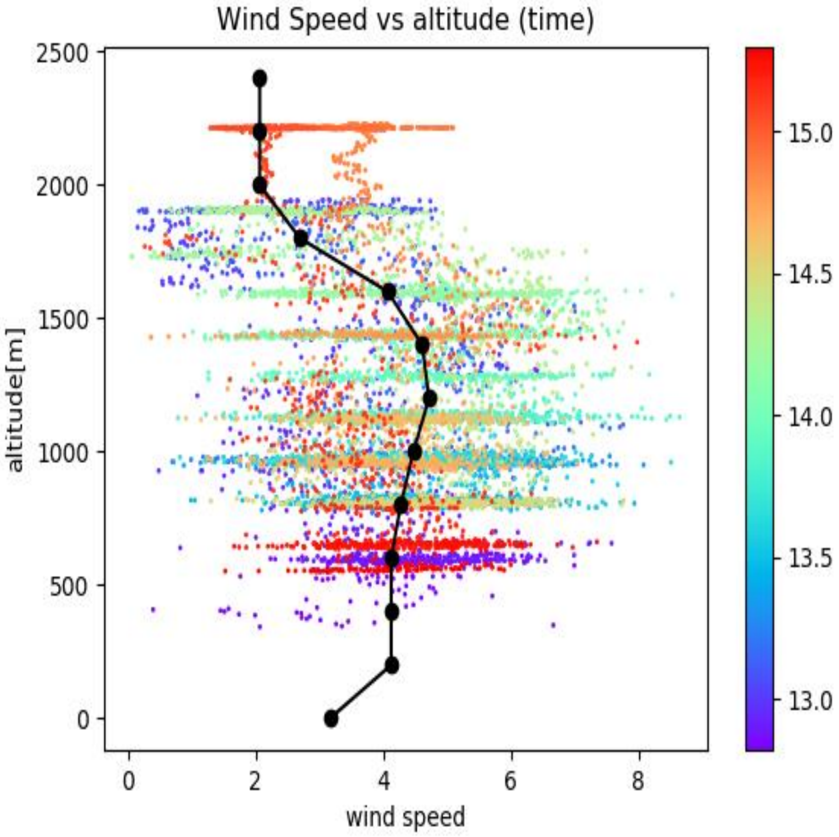

Figure 7: The *in situ* horizontal wind speed from DLR measurements (CoMet flight on 07.06.2018) plotted as a function of altitude above sea level. The colour scale indicates the time of the measurement. The black dots indicate the mean wind speed profile.

The presence of the CO_2 plume from the power plant in the *in situ* measurements is clearly seen in Figure 5 and also in Figure 8 which shows the measured CO_2 as a function of altitude. As seen in Figure 8, the horizontal transects at roughly constant altitude intercept highly elevated values of CO_2. The values from the second ascent taken at a later time further away from the power plant are weaker, as can be expected.

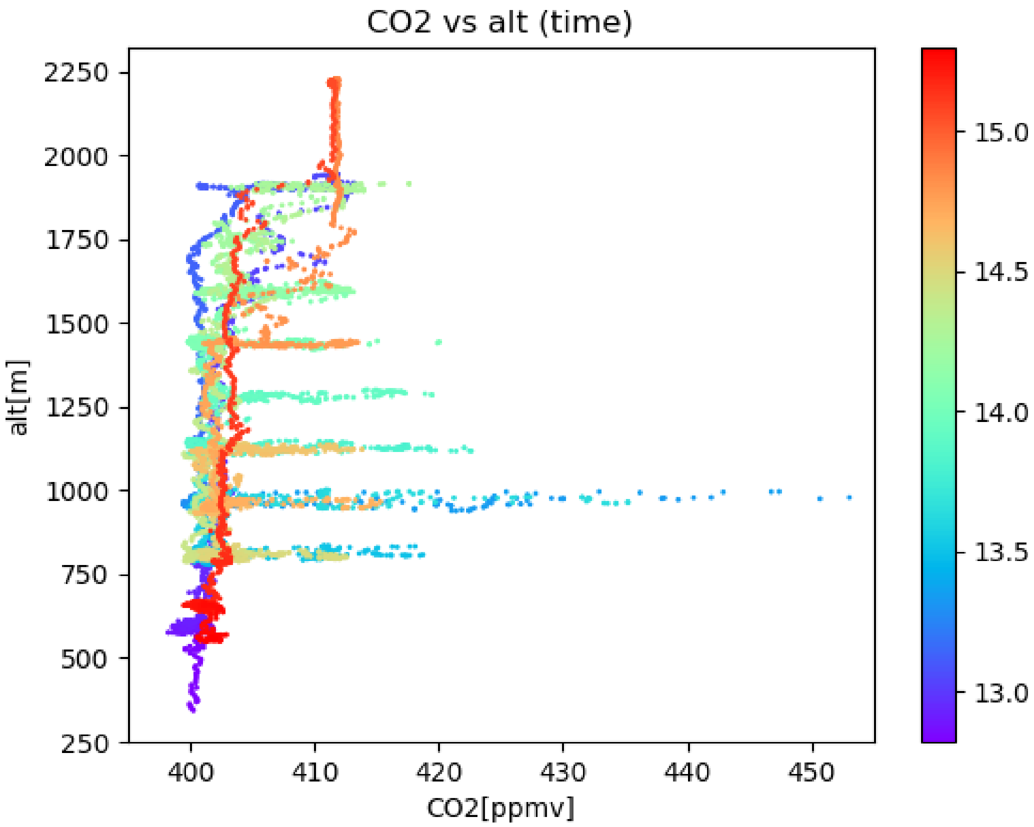

Figure 8: The *in situ* CO_2 from DLR measurements (CoMet flight on 7 June 2018) plotted as a function of altitude above sea level. The colour scale indicates the time of the measurement.

The presence of the CO_2 plume downwind from the stacks is also clearly visible in both MAMAP overpasses (Figure 4).

4.2 Comparison of EULAG output with CoMet observations

4.2.1 Meteorological variables

In this section we compare the wind speed and direction as well as temperature measured *in situ* by DLR with the corresponding simulated EULAG fields. The EULAG fields are interpolated in space and time to the positions and times of the *in situ* observations using the model output saved every 2 minutes. EULAG is initiated and forced throughout the simulations by the meteorological fields from the meso-scale model COSMO-GHG. However, it develops its own circulation inside the domain that is a response to its own model resolution, orographic features and turbulence.

Figure 9 shows the complete time series of the *in situ* measurements (in red) with the corresponding EULAG values superposed (in blue). The time series of the altitude is shown in the top panel to allow the interpretation of the results. The three parts of the flights during which the CO_2 plume was crossed are indicated with brackets: 1) leg from a single pass just downwind from emissions about 6 km from source, 2) leg corresponding to the first progressive ascent of the aircraft to the top of the boundary layer at about 12 km from the source and 3) leg corresponding to the second ascent of the aircraft at about 20 km from the source (see also Figure 3). The aircraft stayed mostly in the boundary layer except on three occasions when it approached or crossed the 2000 m limit (only 2 of these events are in the model domain, see Figure 2). In the free troposphere, as indicated in section 4.1, the wind direction is markedly different from what it is in the boundary layer. EULAG, following the forcing fields of COSMO-GHG, has generally the correct wind speed in the free troposphere, but the wind direction in EULAG is between 180 and 250° while it is between 250 and 300° in the observations. For the transport of the CO_2 plume, it is, however, the meteorological parameters in the boundary layer which are critical. To help quantify the differences between observations and model, we provide Figure 10 which shows the corresponding values as well as the bias plotted as a function of altitude. Panels are provided for wind speed and direction as well as potential temperature.**Error! Reference source not found.** The detailed inspection of Figure 10 shows that the wind direction and vertical shear in the boundary layer are well simulated, even though there is a slight positive bias (not enough northward component in the model) at some altitudes. The simulated wind speed on the other hand is somewhat too high for most of the simulation period and most altitudes. The mean bias reaches 2 m/s at 1400 m. The last sets of panels in Figure 9 and Figure 10 show the potential temperature. The main difference is that potential temperatures in the model are too low by about 2 K in the 800-1200 m layer. As a result of this bias, there is a positive vertical potential temperature gradient in the model while the observations show a relatively constant profile. This difference leads to an increased stability in the model that limits the lifting of the CO_2 plume to the upper part of the boundary layer.

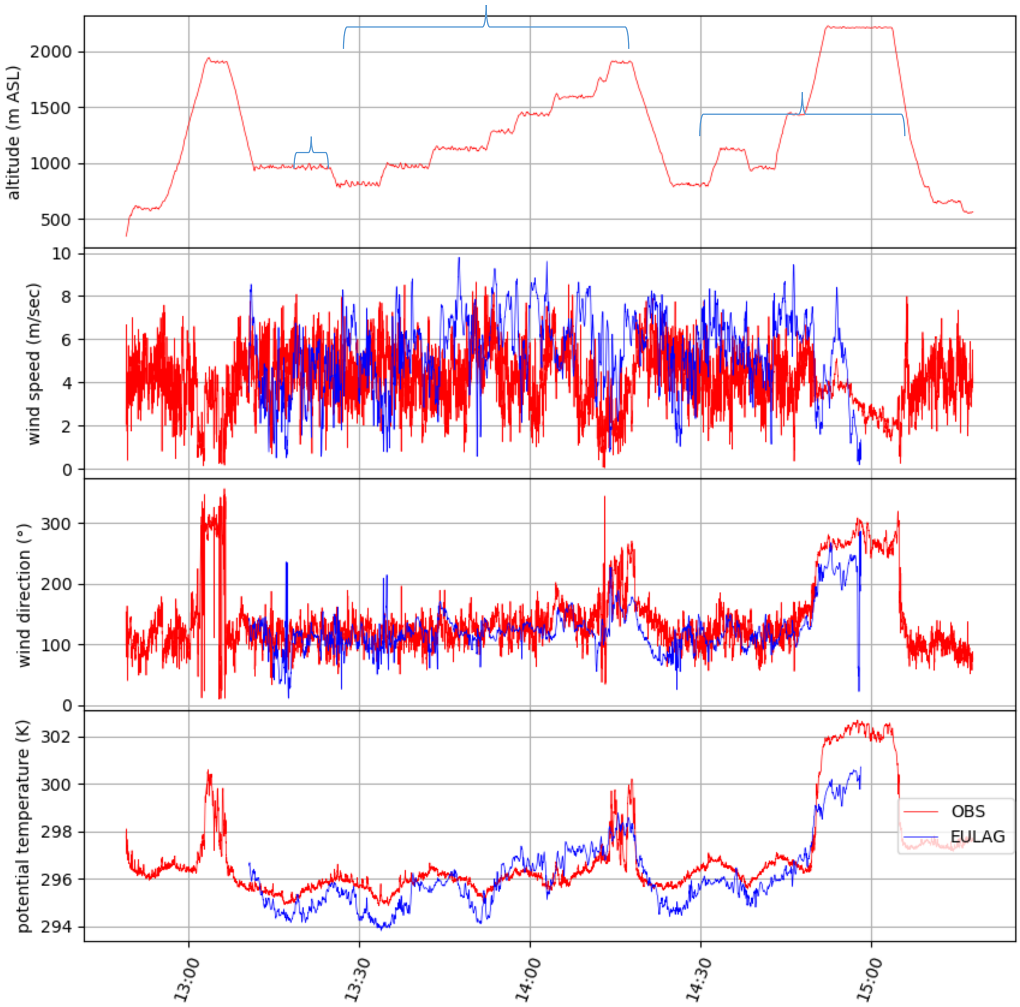

Figure 9: Comparison of wind speed (second panel), wind direction (third panel) and potential temperature (fourth panel) simulated by the EULAG model against the DLR *in situ* measurement (07.06.2018) plotted as a function of time. The top panel shows the measurement altitude. The EULAG values were interpolated in space and time to observation position and time (based on 2-minute output of the model).

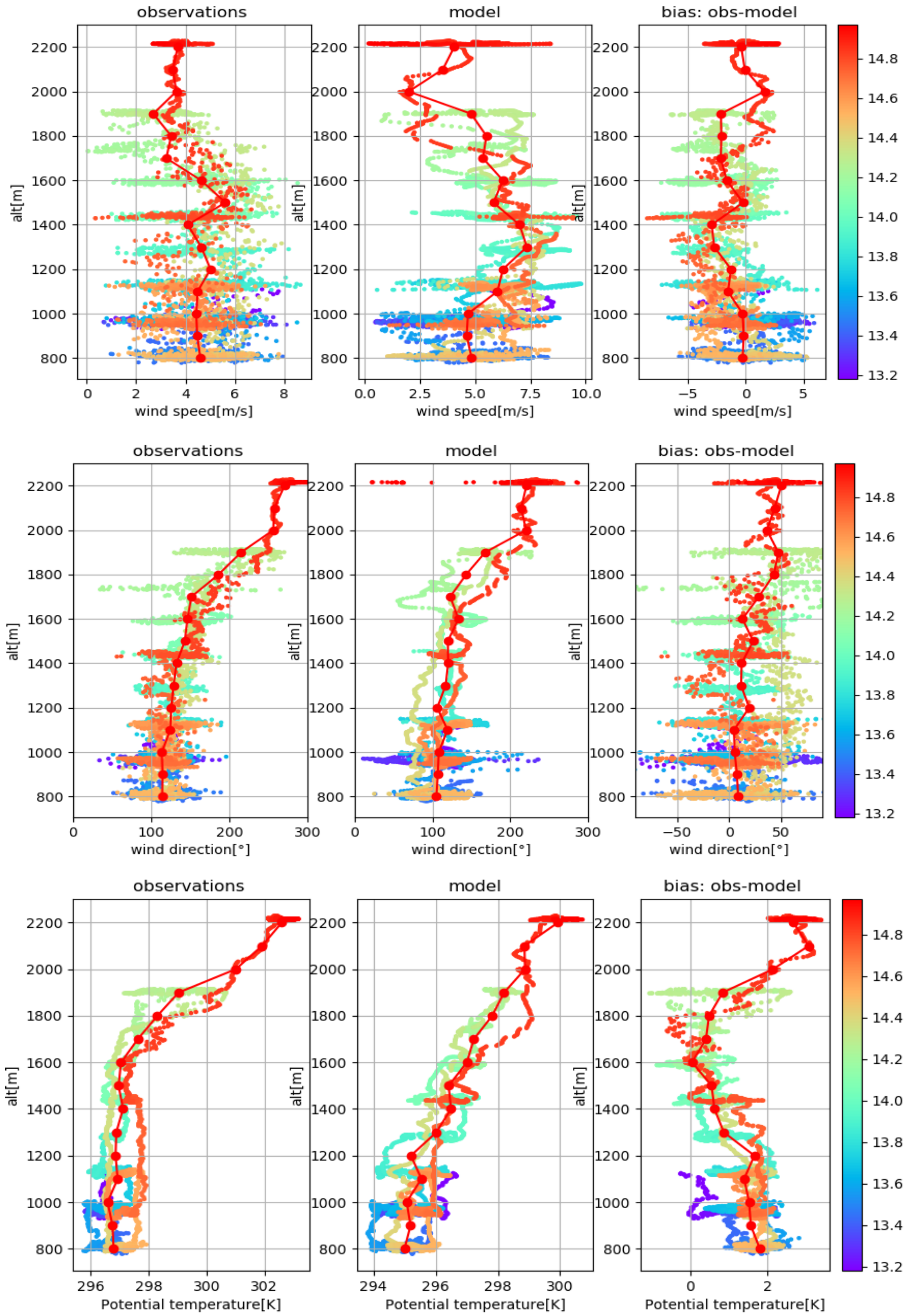

Figure 10: Comparison of wind speed (top panels), wind direction (middle panels) and potential temperature (lowest panels) simulated by the EULAG model against the DLR *in situ* measurement (07.06.2018) plotted as a function of altitude. Each row shows: left panel- DLR observations, middle panel- model, and right panel: model. The EULAG values were interpolated in space and time to observation position and time (based on 2-minute output of the model). The colour of the pixels indicates the time of the measurements. The red dots indicate the mean profile in 100 m bins. Observations are shown only if they fall in the model domain.

4.2.2 CO_2

After the comparison of meteorological fields in section 4.2.1, we focus on CO_2 by comparing the model values against 1) the *in situ* CO_2 DLR measurements and 2) the MAMAP XCO_2 column enhancement data.

4.2.2.1 in situ data

The simulated CO_2 enhancement, which represents the total CO_2 mixing ratios (in ppmv) from both power plant stacks, is compared against the *in situ* values in Figure 11. Note that the model simulates only the CO_2 enhancement, and to compare with observations, the measured boundary layer background of 400 ppmv is added to the simulated values. In the free troposphere, where the background value is larger (e.g. Figure 6), the selected background is inappropriate for comparisons of model values with observations. However, the objective here is to compare the CO_2 enhancement due to power plant emissions rather than evaluate CO_2 mixing ratios throughout the model domain.

Figure 11 shows that the model captures the CO_2 peaks observed during legs 1 and 3 quite well, though the width of the simulated plume on leg 1 close to the stack is too narrow. For leg 2 there is a striking absence of any peaks above 1000 m above sea level (a.s.l.) corresponding to this first aircraft ascent. To understand this difference between observations and model, we show in Figure 12 the model 2D fields at 6 different levels corresponding to the altitudes of the horizontal transects during which the CO_2 plume was crossed by the aircraft (see Figure 8). The figure was plotted for a model output at 14:00. It also contains all measured values, indicated as coloured circles, in the selected altitude ranges for the time interval from 13:44 to 14:00. The figure shows a relatively weak penetration of the model plume above 1000 m, while the observations indicate a fairly wide stretch with values above the background. The weak CO_2 lifting in the model is likely due to the too strong vertical stability discussed in section 4.2.1. This stability is present in particular between 12:30 and 14:00 when there is little penetration of the plume above 1000 m, and the CO_2 accumulates in the lower part of the boundary layer.

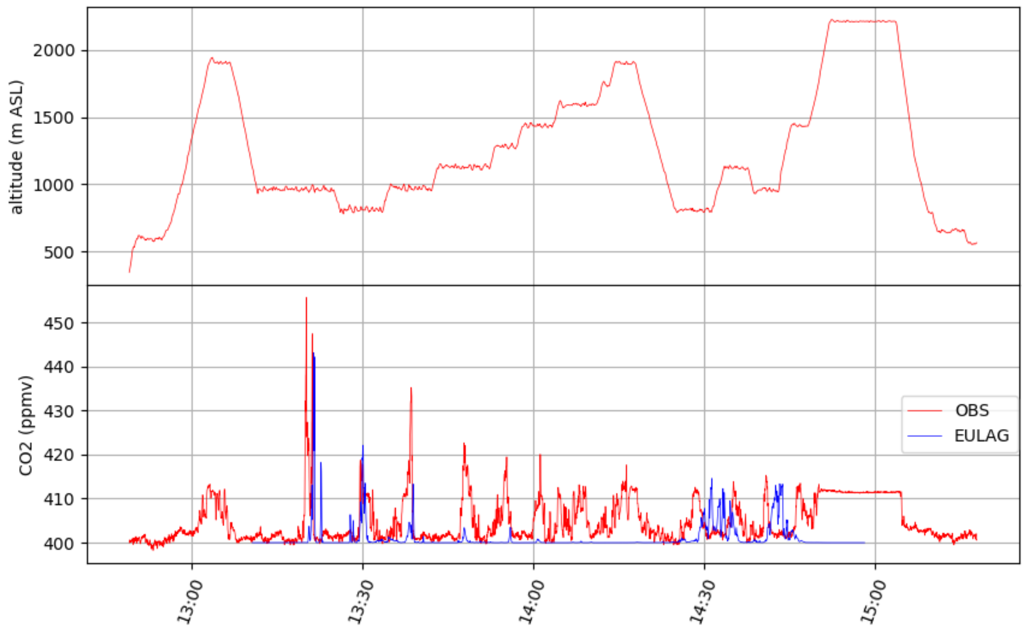

Figure 11: Comparison of CO_2 enhancement (lowest panel) simulated by the EULAG model against the DLR *in situ* measurement (07.06.2018). The top panel shows the measurement altitude. The EULAG values were interpolated in space and time to observation position and time (based on 2-minute output of the model).

Before 12:30 and after 14:00 the lifting of the plume above 1000 m is more efficient as shown for a snapshot at 12:44 (for a lifting episode that took place before 12:30) in Figure 13. The CO_2 that got lifted early in the simulation (i.e. before 12:30) is transported downwind throughout the upper part of the boundary layer.

The reasons for the increased model stability are under investigation and the question was not settled in time for this report. It is believed that this is a result of a model configuration setup rather than model variability affecting plume transport. Our current hypothesis is that the model takes longer than expected to build up its PBL circulation moving progressively away from the COSMO-GHG values (which allow vertical lifting) towards a new equilibrium. For this reason, the vertical lifting takes place only in the beginning and near the end of the simulation. A longer initialisation time could thus be a possible solution. Including the latent heat flux from COSMO-GHG will also impact the temperature profiles. Finally, increasing the model resolution is also under investigation.

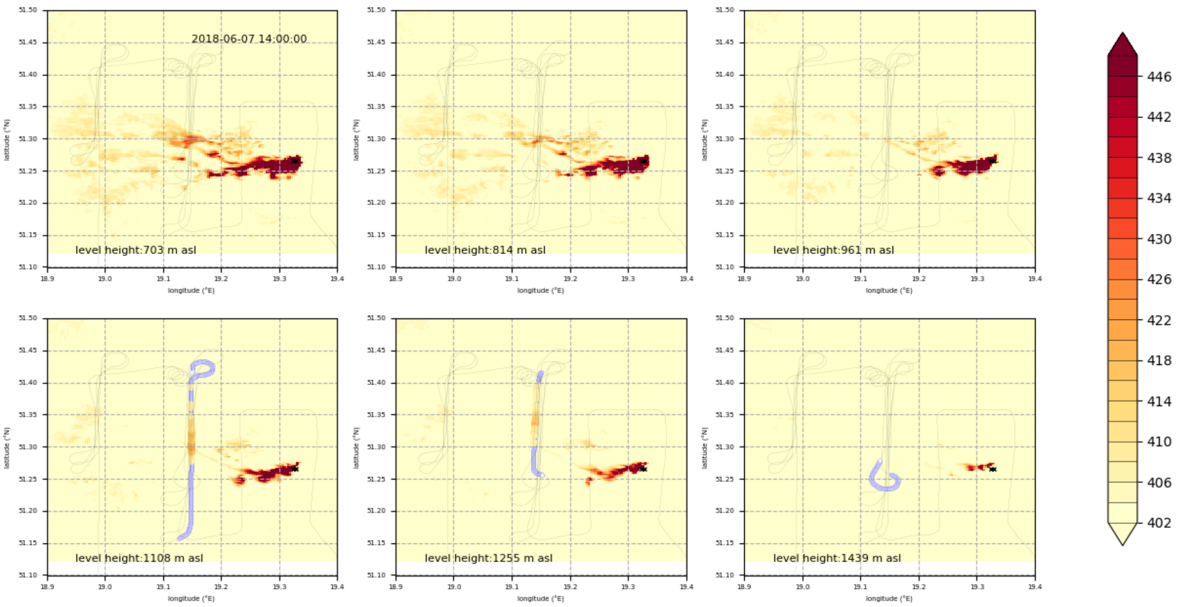

Figure 12: 2D fields represent model CO_2 enhancement at 6 different altitudes above sea level (altitude indicated in each panel) at 14:00 (07 June 2018). The circles indicate the *in situ* measurements between 13:44 and 14:00. The colour of the circles is either white if the measurement is below 406 ppmv (to distinguish from 2D low CO_2 model values) or has the value corresponding to the colour scale for values above this threshold. The observation values are plotted in panels based on the altitude measurement, with the height ranges of each panels being (numbers from left to right starting with top panels): 1- 500 to 757.5 m, 2: 757.5 m to 884 m, 3: 884 m to 1026 m, 4: 1026 to 1184 m, 5: 1184 to 1358 m and 6: 1358 to 1600 m.

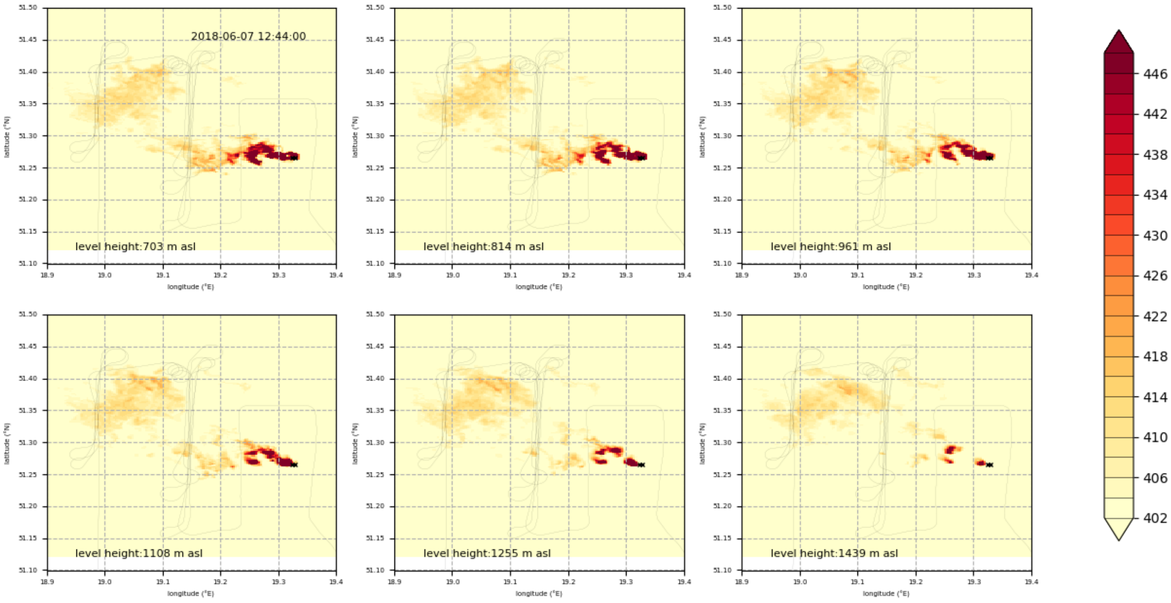

Figure 13 As in Figure 12, but with model data plotted for 12:44 (one hour earlier). There were no *in situ* measurements during the period between 12:30 and 12:44.

To qualitatively evaluate the nature of the plumes generated by the LES model during the time when vertical lifting takes place, we compare the observations against model values shifted back in time by 1 hour and 15 minutes (Figure 14) and by 2 hours (Figure 15). In practice, this is done by subtracting respectively 75 and 120 minutes from the observation times. The shift by 75 minutes leads to a generally proper reproduction of the peaks below 1.2 km. The shift by 2 hours reproduces well the peak location and width for leg 2 below 1.5 km. Above 1.5 km the influence of higher values in the free troposphere can be seen in observations- these values cannot be reproduced with constant model background at 400 ppmv.

This exercise, besides showing the problems with vertical uplifting of the plume during certain time windows due to problems in model setup, also shows the difficulty in comparing directly observed values with a single model run based on a single realisation of turbulent transport. As seen in Figure 12 and Figure 13, and as seen also in mesoscale simulations with COSMO-GHG at 1 km resolution (not shown), the CO_2 transport (on the day analysed here) takes place not within a Gaussian like, continuous plume, but rather as a series of non-continuous puffs that are experiencing the effects of random turbulence. This stochastic nature of the plume transport makes the comparison with high resolution measurements (measurement every 1 second in DLR data) complicated, as one cannot predict exactly the plume/puff pattern and concentration at a given location in space and time. The stochastic nature of transport is analysed in more detail in section 5.

What can be compared between model and observations are the general transport characteristics such as the general width of the puffs (represented by the width of the peaks in the time series plots), the spatial gradients in the puffs, and the absolute values in the puffs.

As expected, the width of the puffs increases, and absolute concentrations decrease, in both model and observations as one gets further away from the emission source. The first observed peak during leg 1 (at about 12:20) in close vicinity to the source shows a pronounced peak of over 450 ppmv. In fact, at the same altitude, there is a secondary peak (best seen in Figure 15) just next to it indicating that there are very high spatial gradients in the observed CO_2. These gradients in observations are also seen in Figure 16 indicating that indeed the pollution is transported during this episode as a series of highly concentrated, non-continuous puffs. The model can also reproduce this two-peak structure as shown in Figure 11, Figure 14 and Figure 15. There is a considerable structure in the observed peak values (for a transect at a given altitude) also further away from the source, as also reproduced by the model and as can be seen in the time series plots and in the 2D plots.

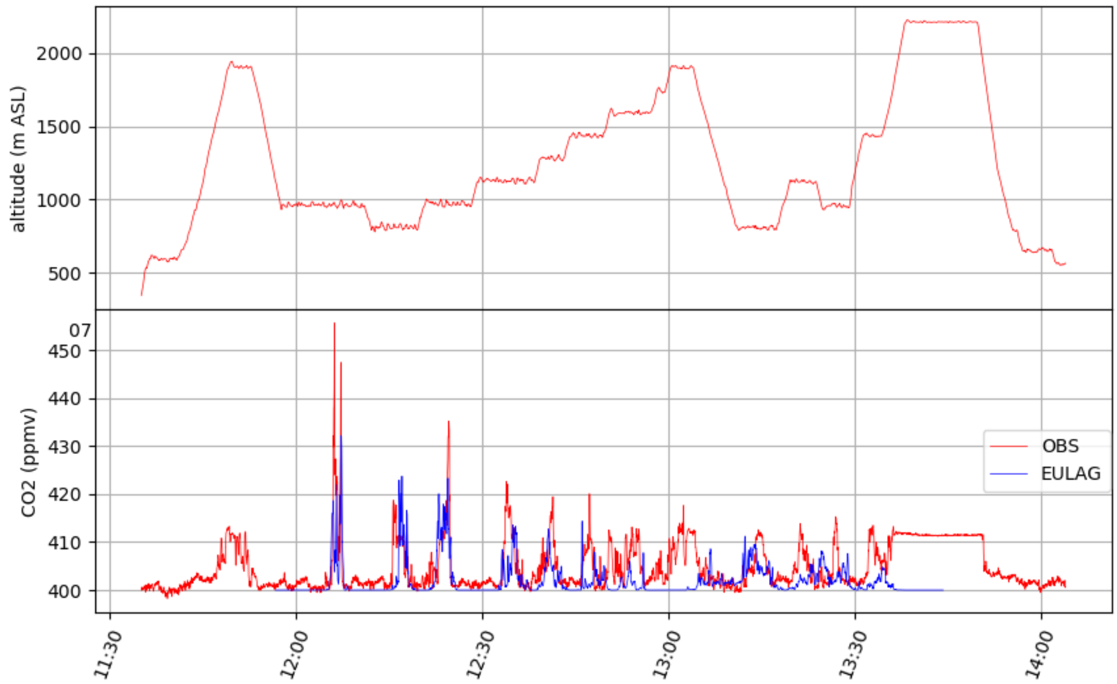

Figure 14: As in Figure 11 but with the observational data shifted in time by -1 hour and 15 min. The model data are extracted for these modified observation times.

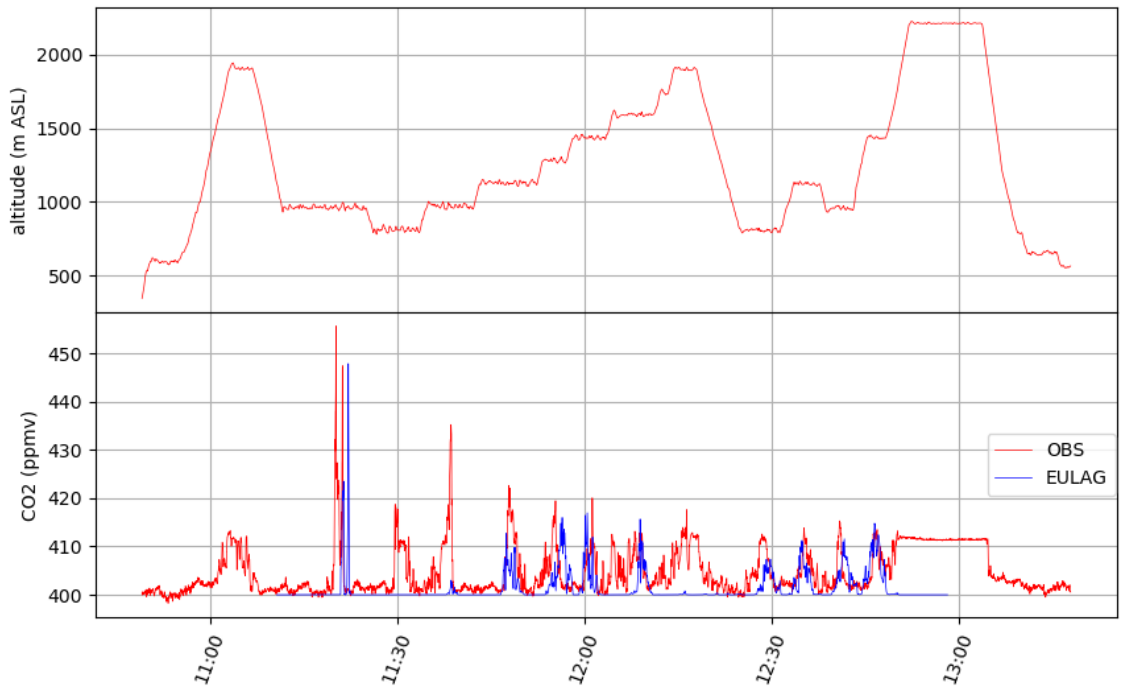

Figure 15: As in Figure 11 but with the observational data shifted in time by -2 hours. The model data are extracted for these modified observation times.

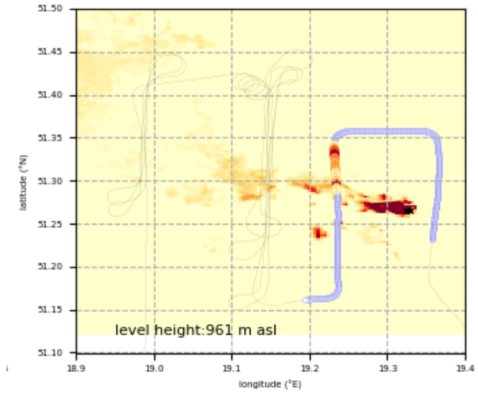

Figure 16: As in Figure 12, but only for one height (961 m) and for 13:30. The observations are plotted for the interval from 13:15 to 13:30.

4.2.2.1 MAMAP enhanced CO_2 column data

In addition to *in situ* measurements, the CoMet campaign provided a unique set of CO_2 total column remote sensing observations. CO_2 column enhancements were measured by the University of Bremen using the MAMAP spectrometer as well as by DLR using the CHARM-F Lidar. Only MAMAP measurements are covered in this report. As presented in section 4.1, the MAMAP data are available from two overflights, called here P1 (12:20-13:27) and P2 (13:27-14:45), that performed measurements on very similar transects.

For comparison with MAMAP total column enhancement (with background data subtracted), the simulated CO_2 values are integrated in the vertical and the resulting columns are interpolated in space and time to MAMAP measurement locations and times. As for *in situ* data, the model data are based on 2-minute output fields. The model results are compared to measured values for flights P1 and P2 in time series plots (Figure 17 and Figure 18) and 2D plots (Figure 19 and Figure 20). The MAMAP observations are performed every 2 s to 3 s. The first transect (called here T0) for both P1 and P2 was upwind from the power plant (see e.g. Figure 19). The model values are strictly zero as there is no CO_2 from power plant at those locations.

As total column enhancements are compared in this section, the problem of insufficient vertical lifting of the plume in the model is less impacting the comparison. However, as seen in section 4.2.1, the plume direction and speed (and possibly other transport characteristics) are dependent on the altitude at which transport is taking place.

Analysis of Figure 17 and Figure 18 indicates that for the transect T1 for both P1 and P2, the model plume has roughly the correct magnitude and width. The observed plume (Figure 19) is crossed earlier and more to the north than in the model, resulting in a slight shift of the simulated peak in Figure 17 and Figure 18. This shift for the model was already discussed for the *in situ* data in section 4.2.2.1 (Figure 11). However, similar to the *in situ* data, shifting model values in time can reproduce the observed distribution. This is shown for P1 for a time shift of -50 minutes in Figure 21 and Figure 22. Similarly, for transects T2 and T3 where single (and too strong) narrow peaks are simulated, a shift in time can lead to wider, double-peaked structures, in better agreement with observations (although the peak values are not exactly those that were observed).

For transects T2 to T7 in both P1 and P2, the model generates relatively well the peak value, but the peak width is generally too narrow. For P1 shifted data the agreement as far as peak width is generally much better, especially for T4-T7. In summary, as for the *in situ* data, 1) matching in time and space observations and model is complicated by the stochastic nature of turbulent transport, and 2) matching better with observations can be achieved by shifting the model data in time indicating that the model can reproduce the observed plume characteristics at different times.

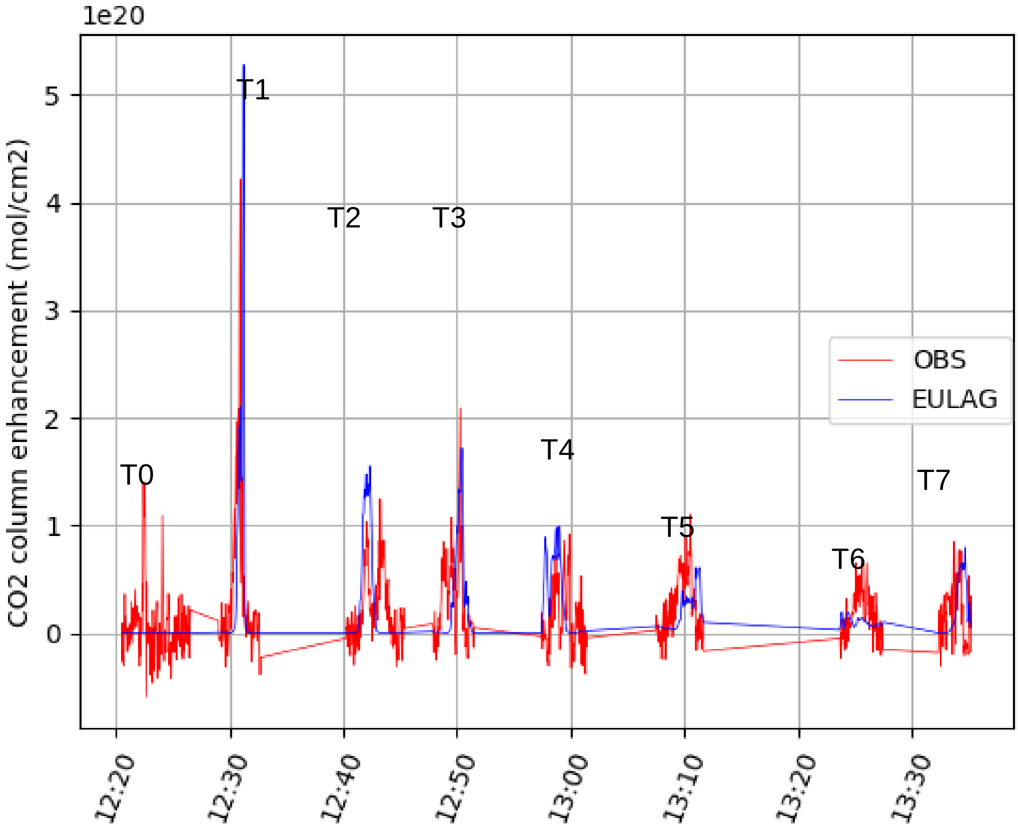

Figure 17: Comparison of CO_2 column enhancement simulated by the EULAG model (blue curve) against the MAMAP measurement (red curve) (07.06.2018) from the first flight P1 (in 10^{20} molecule/cm^2). The EULAG values were interpolated in space and time to observation position and time (based on 2-minute output of the model).

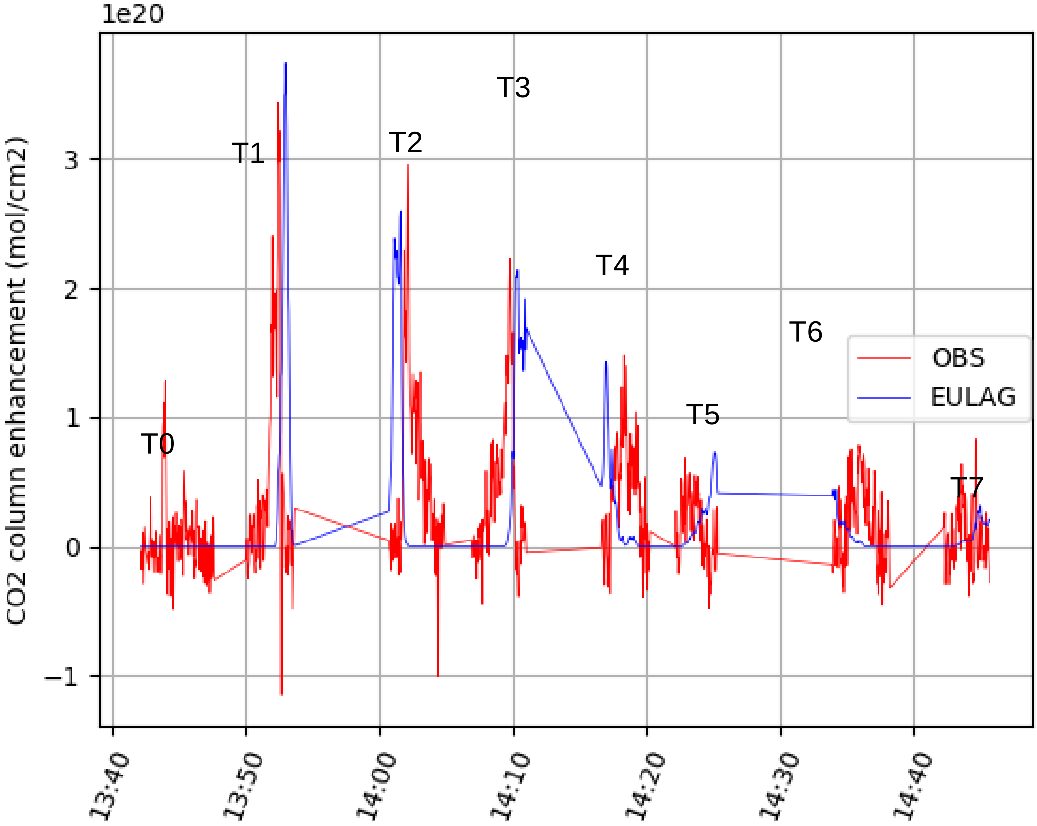

Figure 18: As in Figure 17 but for flight P2. The lines indicate periods with no data.

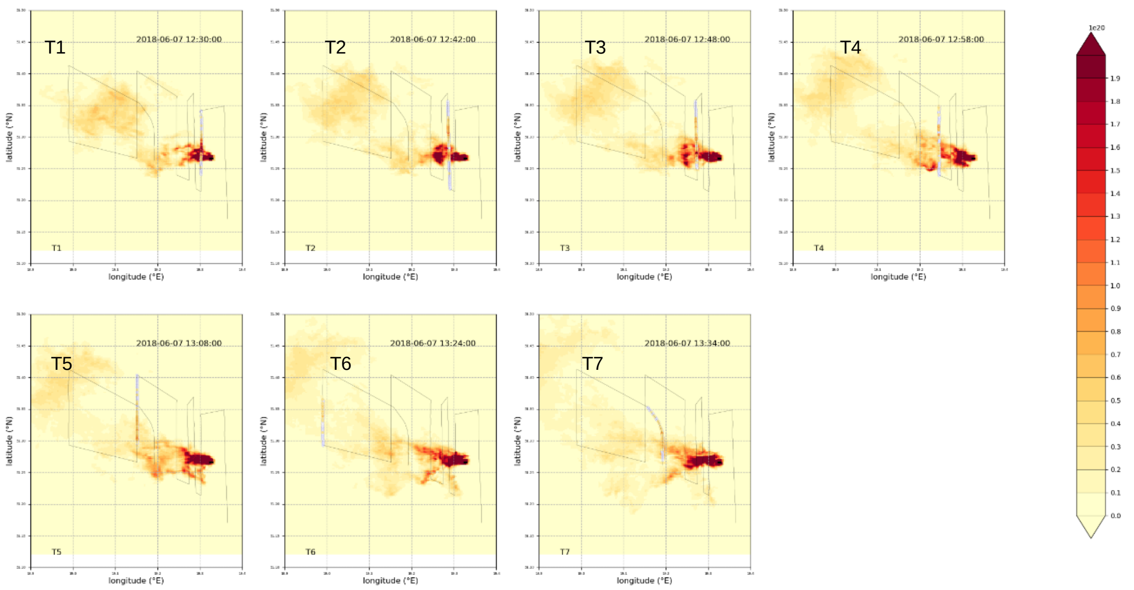

Figure 19: 2D fields represent model CO_2 column enhancement at 7 different times corresponding to the 7 MAMAP P1 transects (mode time indicated in each panel). The circles indicate the corresponding MAMAP measurements. The colour of the circles is either white if the measured enhancement is below 0.25×10^{20} molecule/cm^2 (to distinguish from 2D model values) or has the value corresponding to the colour scale for values above this threshold.

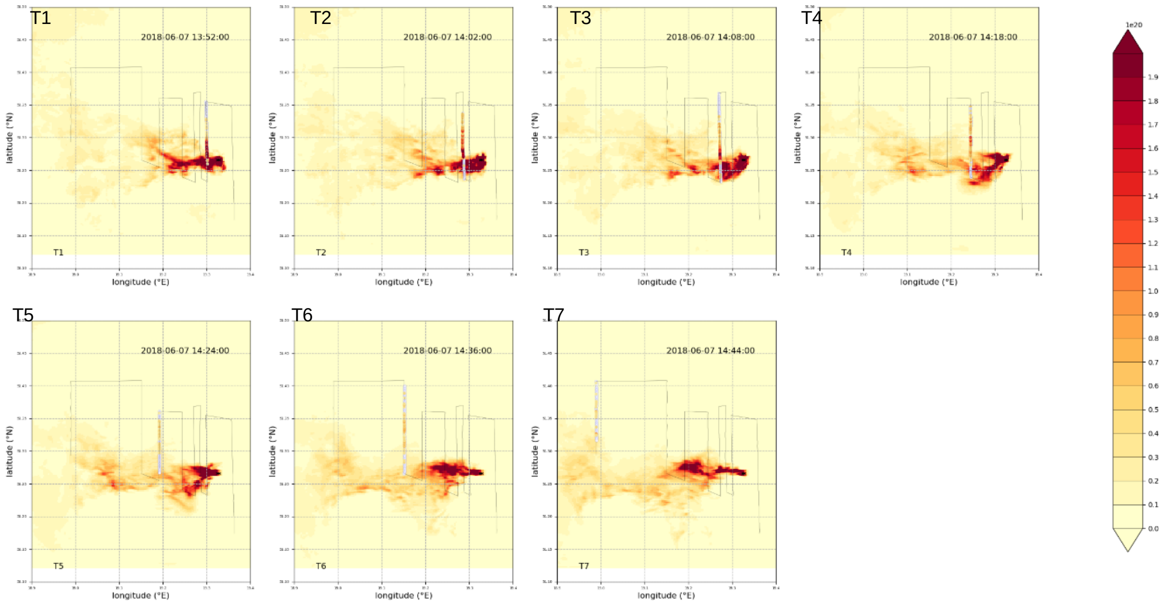

Figure 20: As in Figure 19 but for P2 MAMAP flights

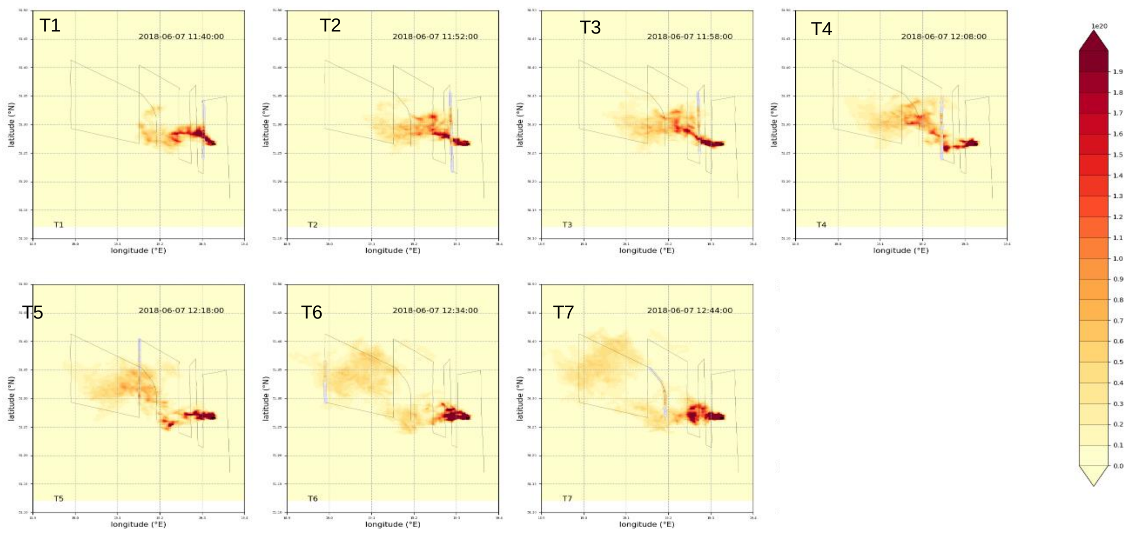

Figure 21: As in Figure 19 for P1 but with observations shifted by - 50 minutes. The model values were extracted for these shifted time values.

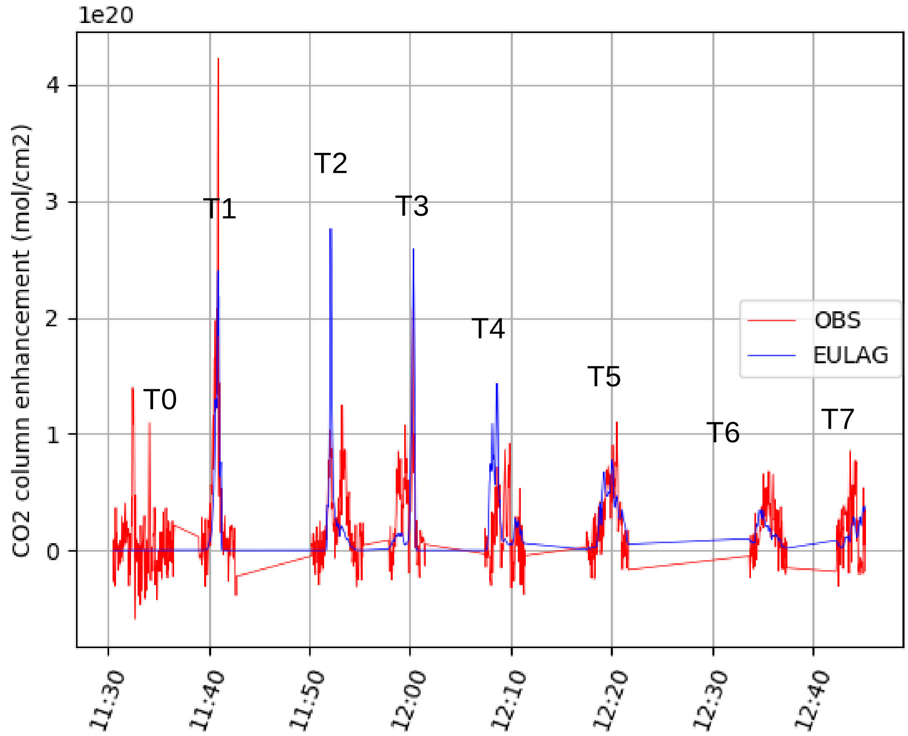

Figure 22: As in Figure 17 for P1 but with observations shifted by -50 minutes. The model values were extracted for these shifted time values.

It is interesting also to note the **temporal** variability in the MAMAP observed plume position between P1 and P2 flights (about one hour apart). For example, for T2, the structure of the peaks is very different between MAMAP P1 and P2 observations, with the P2 peak reaching a maximum close to emission source while for P1 the maximum is reached further north, and the peak is split. For the transects further from the source, the differences between the two overflights are much smaller.

4.3 Summary of the comparison of EULAG results with CoMet data

The EULAG results from simulations forced by the COSMO-GHG output were compared with measured *in situ* meteorological parameters and CO_2 fields from both *in situ* and total column observations.

The wind direction, based on forcing EULAG by COSMO-GHG, is generally well simulated in the atmospheric boundary layer (often noted PBL). On the other hand, the wind speed is generally higher (up to 2 m/s) than the observed values. The modelled potential temperature indicates an increased stability in the upper part of the boundary layer as compared to the observed and also COSMO-GHG profiles. This increased stability limits the plume rising above 1000 m during the 12:30-14:00 period.

The comparison of simulated CO_2 with measured values is impacted by the insufficient vertical lifting, but also by the random nature of the turbulence-driven transport of the highly concentrated CO_2 puffs. Rather than relying only on the 1 to 1 comparison of model vs observations, other criteria need to be applied, such as comparison of the size and strength of the puffs as a function of distance from the source, the horizontal and temporal gradients and the vertical penetration to the upper part of the boundary layer. While the model vertical lifting to the upper part of the boundary layer is too weak during the 12:30-14:00 period, satisfactory penetration of the plume is simulated before 12:30 and after 14:00. Moreover, the qualitative comparison of the puff characteristics (size, peak, gradients) is generally satisfactory as demonstrated by comparison of time shifted data during periods when the model had strong vertical mixing.

5 Preliminary analysis of variability induced by turbulence

As demonstrated in section 4, the model but also the observations, show a high level of spatial and temporal variability. In this section, we try to quantify this variability at different spatial and temporal scales and provide some very preliminary examples to show how this variability impacts flux inversion studies The motivation for this work comes from flux inversion studies in which snapshot observations (e.g. data from polar orbiting satellites such as OCO-2/3 or future CO2M) corresponding to a particular transport situation and plume pattern are used to obtain the information on point source fluxes of CO_2. Due to the stochastic nature of the transport no direct model will be able to precisely represent the transport of CO_2 from point sources to measurement locations. In the retrieval studies using the OEM method, the model uncertainty resulting from this inherent difficulty needs to be estimated and properly considered. Clearly the uncertainty will depend on the size of the measurement pixel, with the relatively large L2 XCO_2 pixels from satellite (e.g. 2 km × 2 km for CO2M) measurements integrating some of the turbulence related features. The situation is different for MAMAP measurements with a resolution of ~50 m that will be more impacted by this uncertainty if individual measurements were used rather than spatial averages. In flux retrieval methods based on mass balance, the non-uniform distribution of XCO_2 will introduce variability in the flux estimates at increasing distance from the point source and at different times. Proper sampling providing a robust mean/average of individual line densities is needed for flux estimates.

The underlying hypothesis here is that the EULAG model with its high-resolution grid of 200 m can serve as a reference representation of realistic tracer transport, with the simulations performed for 7 June 2018 corresponding to a highly turbulent case. We have seen in section 4 that the EULAG model driven by the COSMO-GHG output, while generally able to reproduce the observed features of CO_2 transport (in its current setup) does not have enough vertical penetration of the plume into the upper part of the PBL during a significant part of the simulation period. There might be other important limitations of the current model setup. Nevertheless, we proceed with the analysis of the impact of variability on flux retrieval methods using the present setup of the EULAG mode. This analysis will be repeated in the future with an improved setup that could better reproduce the vertical stability.

We start the analysis in section 5.1 by analysing the spatial variability (§5.1.1) and temporal variability (§ 5.1.2). In section 5.2 the impact of this variability on flux retrieval methods is discussed.

5.1 Analysis of spatial and temporal variability in the EULAG results

5.1.1 Spatial variability

The EULAG model was run at the spatial resolution of 200 m. We degrade the model resolution (with pixels at (i,j)) by aggregating the neighbouring pixels and calculating the sliding mean XCO_2 values. For 1000 m resolution, all pixels in the range (i-2:i+2, j-2:j+2) are included in the average, for 2200 m all pixels in the range (i-5:i+5, j-5:j+5), etc. The images of the XCO_2 plume at 4 spatial resolutions (200, 1000, 2200 and 4200 m) are shown in Figure 23. As the resolution is degraded, the small puffs get averaged, and the spatial gradients and peak XCO_2 values decrease. With reduced resolution the plume starts resembling a Gaussian plume shape. There are, however, even at 4200 m, two maxima that can be seen as 2 large scale puffs, one just downstream from the emission points and another at about 30 km in the NW direction. The presence of two maxima indicates distinctly different behaviour than a simple

Gaussian dispersion. Using a simple Gaussian model could lead to flux estimation errors for this case. This error could be estimated by generating pseudo-observations from the simulated LES values and performing the flux inversion.

The spatial standard deviation is significant as shown in Figure 24 and can be higher than 50% (Figure 25). The relative variability is especially high near the emission source where very strong spatial gradients exist. The presence of this spatial variability can be also seen in the CoMet MAMAP column enhancement measurements (Figure 17 and Figure 18) and also in *in situ* DLR measurements (Figure 11). Having measurements at coarser resolution (i.e. from satellite instruments) allows to average a significant fraction of this variability and considerably increase the size of the puffs.

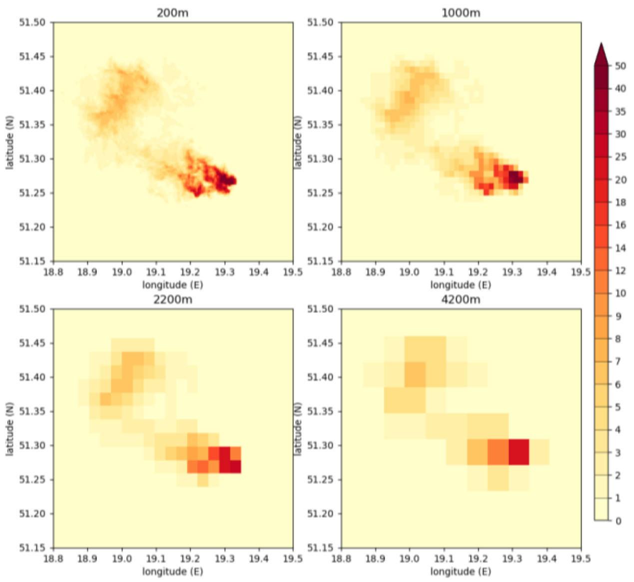

Figure 23: Impact of spatial resolution on the simulated XCO_2 plume enhancement (in ppmv) at 13:00 (07.06.2019): top left – original EULAG resolution of 200 m, top right – 1000 m, bottom left – 2200 m and bottom right – 4200 m.

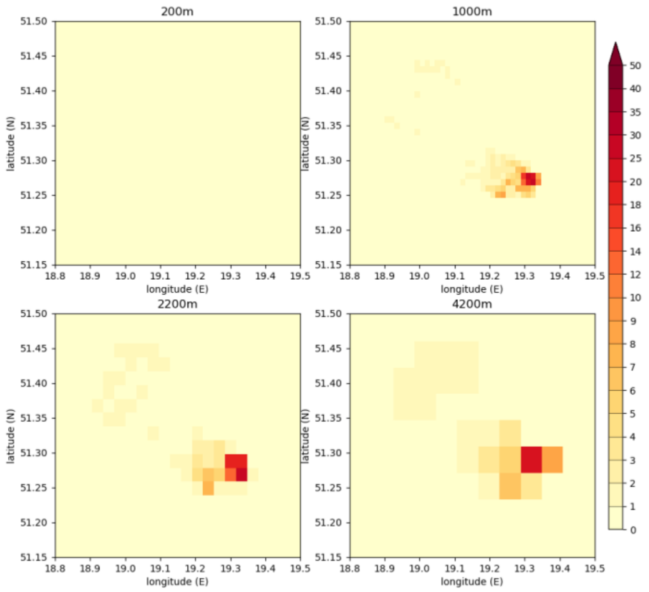

Figure 24: As in Figure 23, but the spatial standard deviation of XCO_2 is shown (in ppmv, standard deviation considering the individual 200 m pixels within the 1000, 2200 and 4200 m grids).

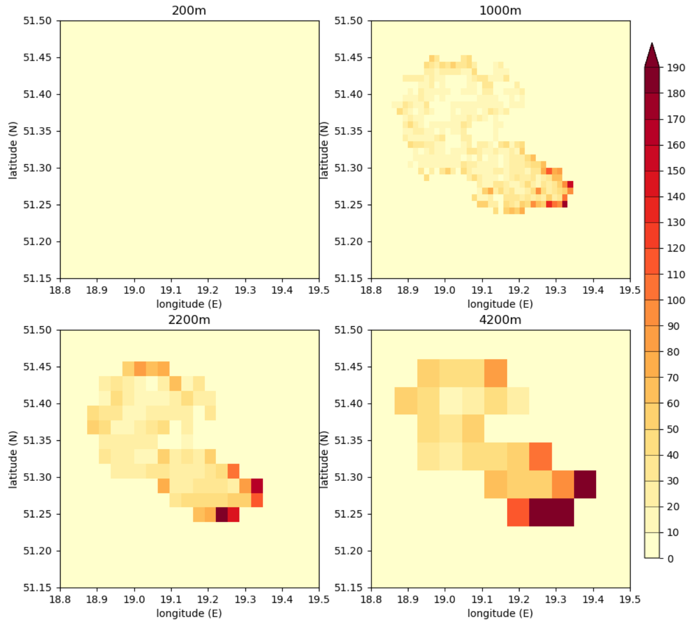

Figure 25: As in Figure 23, but the ratio of spatial standard deviation of XCO_2 to corresponding spatial mean is shown (in %). Only pixels with mean value of > 1 ppmv are shown.

5.1.2 Spatio-temporal variability

In addition to the spatial variability, when considering the transient nature of puff advection, one needs to also consider the temporal variability. Polar orbiting satellites for example can provide measurements during a very limited temporal window that represents a snapshot of a given plume during the satellite overpass. Under turbulent conditions, the plume shape might be different than the generally assumed static Gaussian plume. Any flux inversion studies based on individual overpass should account for this source of uncertainty.

It is the goal of this sub-section to estimate this uncertainty based on LES high-resolution model results. This uncertainty is quantified for boxes of different sizes – as seen in section 5.1.1, larger grids are averaging/smoothing some of the spatial structures of the simulated plume.

It is important to note that in this temporal analysis the meteorological conditions remain relatively stable and the temporal variability is due to the transit of non-homogenous features of the puff rather than (for example) major wind direction changes.

We start by showing, as in section 5.1.1, three figures with:

1. mean values
2. standard deviation
3. ratio of standard deviation and mean value.

Each figure contains results for four different resolutions: 200 m (original), 1000 m, 2200 m and 4200 m. Unlike in section 5.1.1, where the statistics are calculated for a single time step based on 200 m pixels, here the standard deviation is calculated based on temporal samples corresponding to values at given times for a given grid size. In the figures shown below, the statistics is done on 30 time steps for the period between 13:00 and 14:00 (model output every 2 minutes). The period between 13:00 and 14:00 was chosen since during this period the plume is already well established in the domain and the plume direction stays constant (wind from south-east).

Figure 26 with temporal means indicates the presence of fairly diffused features (in comparison to the output for a single time step in Figure 23) due to the advection of the puffs in time. The standard deviation close to the source is smaller than in Figure 24, indicating that there is more variability due to spatial averaging of small features than to temporal averaging (near the source the concentrations are generally high during the entire period). Further away from the source, the contrary is often true with a stronger temporal variability (the variability due to the displacement of the puffs leads to stronger gradients than the variability within puffs). The ratio of standard deviation to mean shown in Figure 28 indicates generally elevated values, with highest values on the edges of the plume (low mean and high standard deviation).

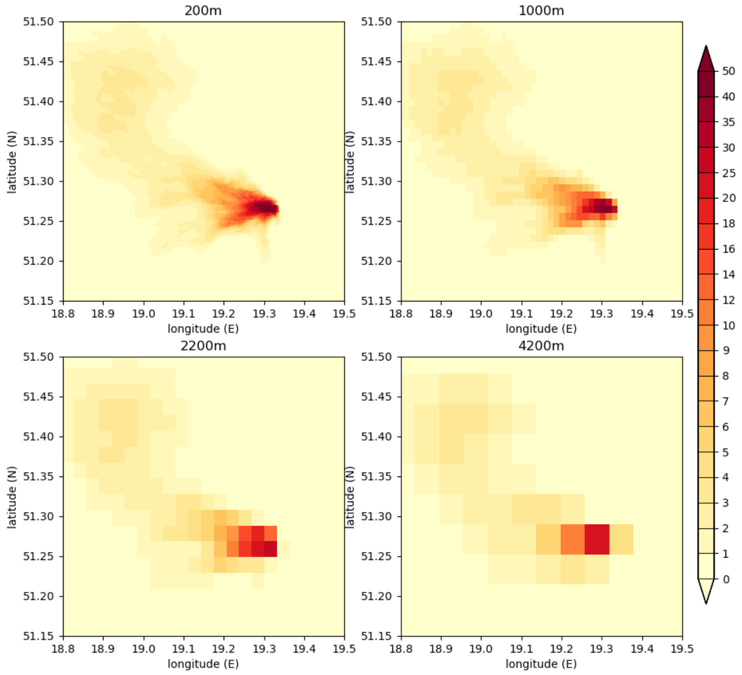

Figure 26: Mean XCO_2 column enhancement simulated by the EULAG model during period from 13:00 and 14:00 (7 June 2018, average over 30 model time steps) for 4 different spatial resolutions

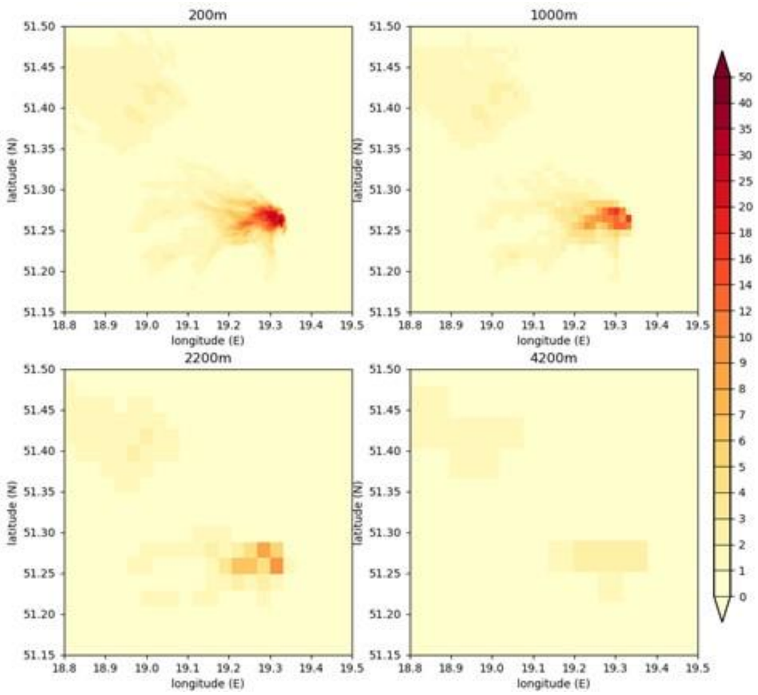

Figure 27: As in Figure 26, but the temporal standard deviation of XCO_2 is shown (in ppmv, standard deviation considering the pixels at 200, 1000, 2200 and 4200 m resolution over the 1 hour period from 13:00 and 14:00).

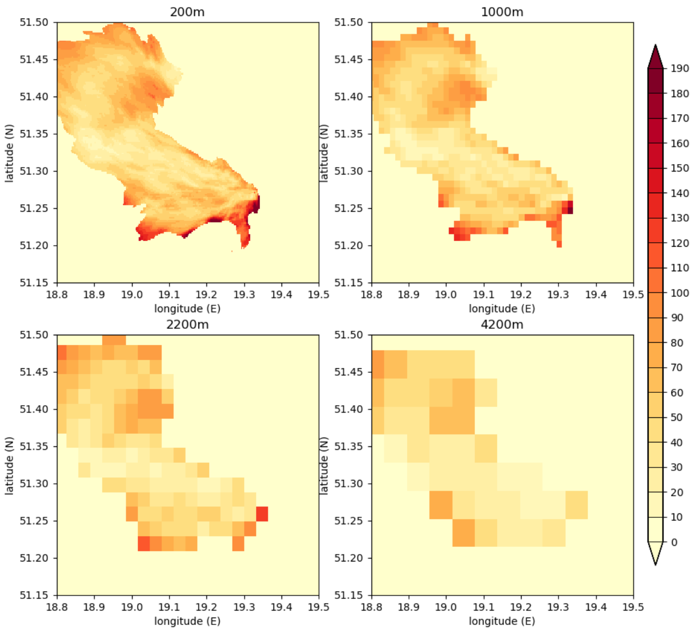

Figure 28: As in Figure 26, but the ratio*100% of temporal standard deviation of XCO_2 to temporal mean XCO_2 is shown. Only pixels with XCO_2 mean above 1 ppmv are shown.

5.2 Applications of the analysis of LES variability on flux retrievals methods

In section 5.1 we have characterised the spatio-temporal variability in the LES results due to the turbulent, non-Gaussian behaviour of the plume transport. This analysis was performed for the highly turbulent case on 7 June 2018. In this section, we provide some very preliminary analysis of how these results could be used in the two flux retrieval approaches: the OEM based method in which an optimal solution is searched by minimising the cost function (containing generally two terms: one for the difference between optimised forward model simulated field and observations and the second between the optimised model result and *a priori)*, and the second approach based on mass balance analysis in the plume.

5.2.1 Quantification of the variability – for retrieval based on OEM methods

Scatter plots of all means (Figure 26) vs standard deviations (Figure 27) for the 13:00 - 14:00 period are shown for four grid resolutions in Figure 29. The linear least squares regression between means and standard deviations is calculated with the intercept at 0 by design. The slope of this regression line can be calculated with the following formula:

$$slope = \frac{\sum(y_i \times x_i)}{\sum(x_i \times x_i)}$$

where y_i corresponds to the temporal standard deviation for a given pixel at a given spatial resolution and x_i is the corresponding mean. The slope is clearly decreasing with increasing pixel size. At the coarsest resolutions (but also to some extend for 1000 m pixels) one can distinguish points that have an elevated mean and a low standard deviation. This mode corresponds to pixels englobing the source (with the sliding spatial mean in x and y directions there is a significant number of such pixels) or close to it. As discussed above, these points have relatively low variability as the column values stay high due to the proximity of the source.

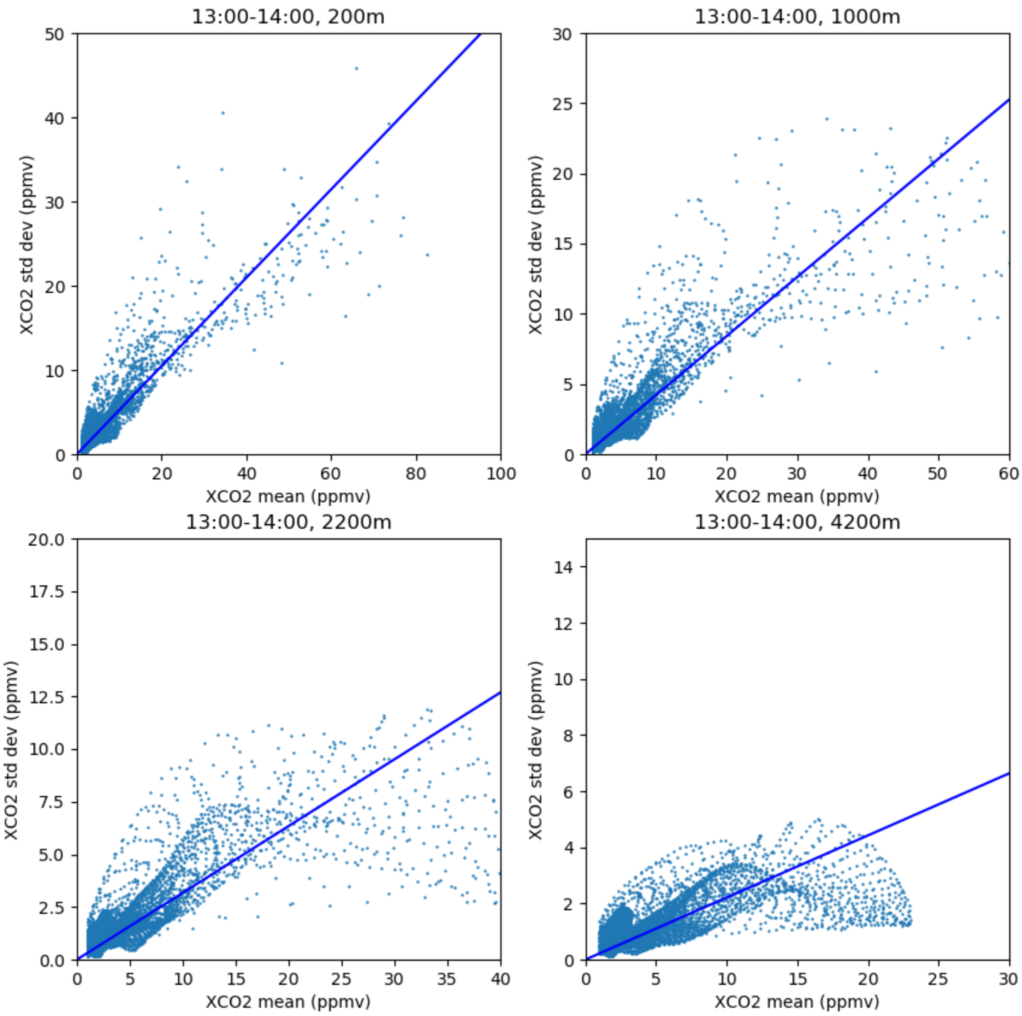

Figure 29: Scatter plot of mean XCO_2 column enhancement vs corresponding temporal standard deviations based on values simulated by the EULAG model during period from 13:00 and 14:00

(7 June 2018, average over 30 model time steps). The line corresponds to the linear regression with intercept at 0.

The impact of the pixel size on the regression slope is shown explicitly in Figure 30 (for the 30 time steps in 13:00-14:00 model output). The relative variability decreases from over 50% at the 200 m resolution to just over 20% at 4200 m resolution. This relative variability could be used as a first estimate of the uncertainty due to the inherent difficulty of reproducing the pattern of turbulent features by a forward model used in the OEM approach. This uncertainty is provided at pixel level. As CO_2 transport takes place in puffs rather than individual pixels, the impact of spatial correlation between pixels will lead to reduction of these estimates.

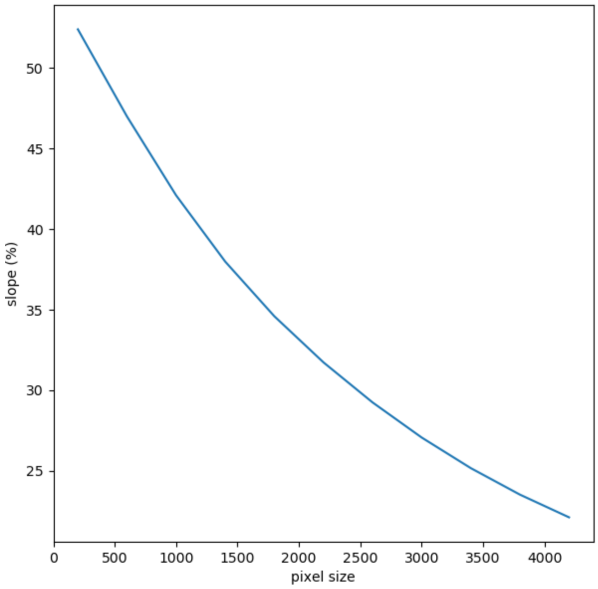

Figure 30: Slope of the linear regression (in %) for temporal sampling shown as a function of pixel size for 30 time steps in the period 13:00 - 14:00 .

5.2.2 Impact of variability on the mass balance flux retrieval methods

The utility of the mass balance approach for retrieving surface CO_2 fluxes was recently demonstrated by Kuhlmann *et al*., [2019]. The approach was applied to the emissions of the city of Berlin using synthetic observations based on COSMO-GHG simulations with L2 specifications corresponding to the CO2M mission currently under preparation by the European Commission and the European Space Agency (ESA). The authors show, that depending on the scenario chosen, i.e. the CO_2 level 2 product error, the ability to identify the plume (with and without the simultaneous NO_2 measurements that help to identify the exact plume pattern) and the CO_2 background, the method when applied to CO2M measurements should lead to annual flux estimation for a city like Berlin with a precision of 10 to 20%.

The line densities in the Kuhlmann *et al*., [2019] approach are estimated for several quadrilaterals positioned along the plume at different distances from the emission source (see e.g. figure 1 and 4a in Kuhlmann *et al*., [2019]). For each quadrilateral, the flux is estimated based on integration of available observations. Based on Kuhlmann *et al*., [2019]:

$$M_p(x_p) = \int_{y_{min}}^{y_{max}} c_p(x_p, y_p) dy_p$$

- were $M_p(x_p)$ is the estimated line density for a given quadrilateral with units of kg/m
- x_p and y_p are the coordinates along and across the plume direction, respectively,
- y_{max} and y_{min} are the integration limits in the across plume direction and
- $c_p(x_p,y_p)$ is the plume signal in kg/m^2 (with background removed).

For each polygon, the flux is obtained by multiplying the line density by the wind speed perpendicular to the plume direction. The final flux for a given overpass is obtained by averaging the estimations obtained from several polygons (up to 50 km from the plume source).

In Kuhlmann *et al*., 2019, the integration to obtain the line densities is done with two methods: one using the individual measurements and the second using a Gaussian fit to these measurements. In the present deliverable, the method based on individual measurements is used. In its implementation, in order to prevent the missing pixels from influencing the results, as in Kuhlmann *et al*, 2019, the integration is done by first calculating mean value for slabs positioned in the across plume direction (e.g. slabs of 5 km width) and then the line densities for each slab are summed up.

Figures 4b and 5b in Kuhlmann *et al*. 2019 indicate that for the flux estimations applied to the tracer containing only the CO_2 from Berlin, the variability between estimations made for different polygons with increasing distance from the source is relatively weak. The variability is increasing considerably for CO_2 including all sources and sinks (including other industrial and biogenic sources/sinks) due to the difficulty in precisely estimating the Berlin contribution to the total plume (c_p).

In the present work we look at the spatio-temporal variability in the line densities using the high resolution LES model applied to a strong point source. It is expected that the city emissions coming from a multitude of sources over a large area will be more diffused and less prone to a puff like transport that leads to high variability. We apply the Kuhlmann *et al*. 2019 approach with several simplifications: 1) we consider only the CO_2 coming from the Bełchatów power plant so the background is fixed at 0 (this corresponds to the noise free model tracer), 2) the plume direction is assumed to be linear (a straight line) rather than a curve.

The plume direction is determined by performing a linear regression weighted by the CO_2 column. The integration is done for rectangles of fixed width in the along plume direction and using slabs in the across plume direction for which mean values are calculated before integration.

We investigate how the presence of turbulence derived plume features is impacting the spatio-temporal values of the calculated line densities. This work is only preliminary and will be pursued after the submission of this document.

To test the developed analysis package, we apply it first to a Gaussian plume for which it is expected that the line densities are constant as a function of distance from the source. The simulated columns as well as the polygons used for calculating line densities are shown in Figure 31a. A flux F of 38 MtonCO_2/yr, a wind speed of 5 m/s and a stability factor of 213 were used for the definition of this Gaussian plume under unstable conditions (Krings *et al*., 2011). The estimated line fluxes (line densities multiplied by wind speed) are shown in Figure 31b for a set of rectangles of 2 km width with increasing distance from the source. The estimated flux values for all rectangles are very close to value used to define the Gaussian plume and the variability between the individual estimates is very low. The mean value over 14 rectangles is 37.93 MtonCO_2/yr.

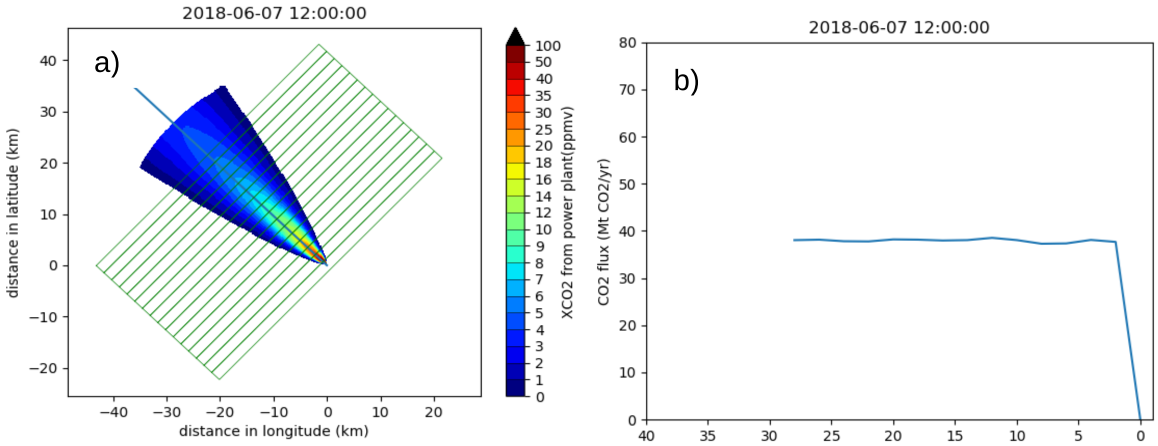

Figure 31: Mass balance retrievals for a Gaussian plume with u=5 m/s, a=213, flux=38 MtonCO$_2$/yr, angle of 45°, 14 rectangles of 2 km width and slabs of 5 km. a) the corresponding XCO$_2$ columns (ppmv), b) the corresponding fluxes for each rectangle (in MtonCO$_2$/yr).

After this preliminary setup validation, we apply the method to the LES simulated plume at 14:00 UTC (7 June 2018).

Figure 32a shows the corresponding model XCO$_2$ with the plume direction indicated by the regression line. The non-Gaussian nature of the plume is apparent with the presence of numerous local maxima. Based on mean wind speed in Figure 10, the wind speed of 5 m/s, which corresponds to the mean boundary layer speed, is taken. The plume direction is indicated by the regression line, but with the puffs moving in different directions this direction can be taken as best as the mean direction of the displacement of CO$_2$. The total CO$_2$ column enhancement (in kg/m^2) is integrated for each of the rectangles (2 km width) shown in Figure 32a. As in Kuhlmann *et al*.; 2019, and as explained above, each of the rectangles is divided into slabs, for which a mean column is calculated. The total value for each rectangle is a sum of the slabs. The length of the slabs used here (perpendicular to the plume direction) is 5 km. Figure 32b shows the corresponding estimations of the line densities multiplied by the assumed wind speed for different distances from the source. The value of the flux averaged over 14 rectangles (28 km) is 43.9 MtonCO$_2$/yr. The values are higher than the emitted flux of 38 MtonCO$_2$/yr at less than 10 km from the source, and generally close to the expected value at more than 10 km from the source. The too high values are linked to the fact that transport with the current LES setup often takes place too low in the boundary layer, with highest concentrations often close to the surface (especially close to source) where the wind speed is much lower than the mean boundary layer speed. Using 5 m/s for converting line densities into fluxes is thus not fully justified. A simple exercise in which the line densities and resulting fluxes are calculated only above level 10 (above 400 m above surface) gives a total flux of 21.3 MtonCO$_2$/yr thus demonstrating that indeed a major part of the flux calculated in Figure 32b takes place close to the surface. In this situation, not only the mean speed is often lower but also the wind direction is more variable, further reducing the wind speed in the assumed plume direction. This example shows the difficulty of applying this method when the plume transport takes place at different altitudes with different wind characteristics.

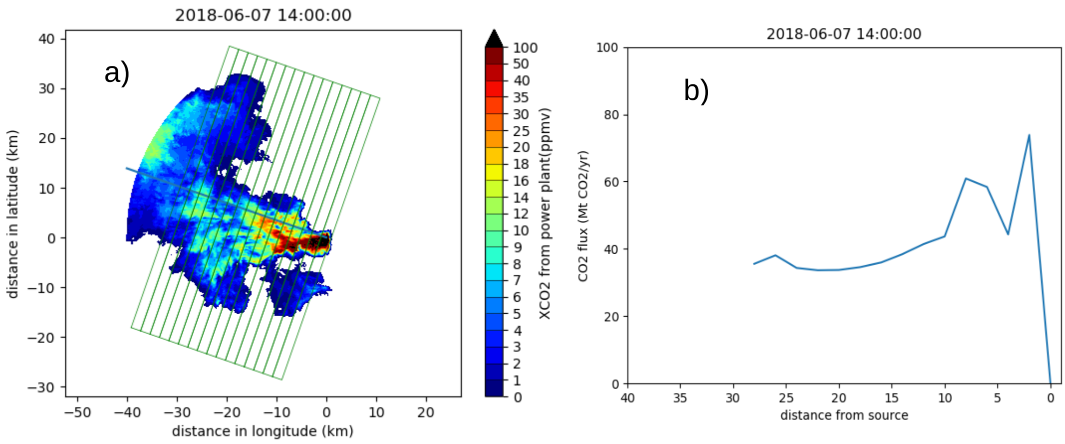

Figure 32: Mass balance retrievals for a LES plume at 14:00 UTC (7 June 2018) with surface flux=38 MtonCO_2/yr, 14 rectangles of 2 km width and slabs of 5 km. a) the corresponding XCO_2 columns (ppmv), b) the corresponding fluxes for each rectangle (in MtonCO_2/yr).

Next, the exercise has been repeated for 16:00 UTC when a large part of the plume is lifted to altitudes higher than 1000 m. The resulting plume shown in Figure 33a is moving now in the westerly direction, still with a complicated plume structure. As before, the wind speed of 5 m/s is taken as the mean wind speed for converting line densities into fluxes.

The resulting values are similar to the ones at 14:00, with the mean value at 45.9 MtonCO_2/yr. About 20 % of the transport still takes place in the lowest 400 m. As a validation exercise, one can use the actual wind speed in the direction of the assumed plume direction (calculated by performing a dot product between model wind (u,v) and a unitary vector in the direction of the plume) at each model level and each model pixel. The corresponding Figure 34 shows values smaller than with fixed wind speed with a mean at 34.8 MtonCO_2/yr. This value is smaller than the input value, possibly because the plume is moving also in other directions (with somewhat higher wind speed than the wind speed projected on the assumer wind direction).

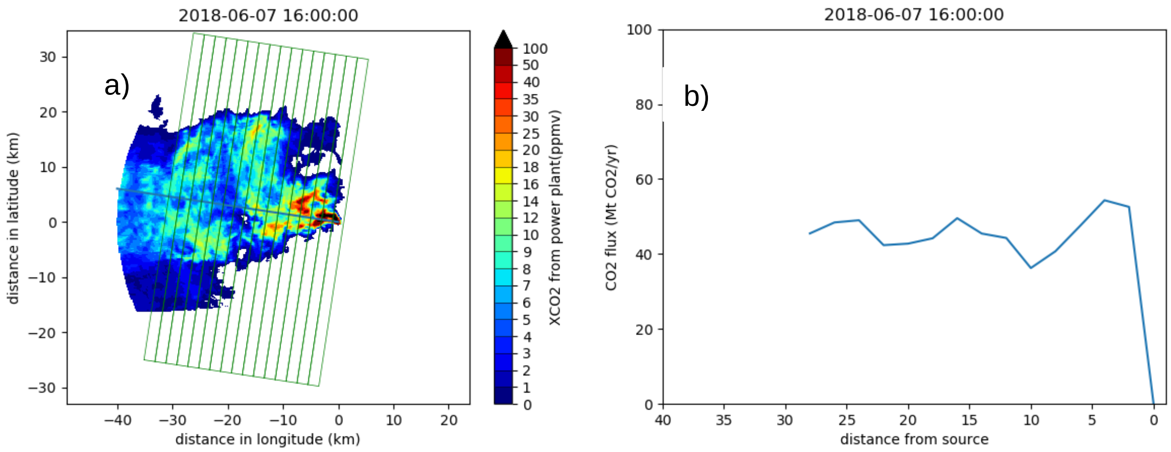

Figure 33: Mass balance retrievals for a LES plume at 16:00 UTC (7 June 2018) with surface flux=38 MtonCO$_2$/yr, 14 rectangles of 2 km width and slabs of 5 km. a) the corresponding XCO$_2$ columns (ppmv), b) the corresponding fluxes for each rectangle (in MtonCO$_2$/yr).

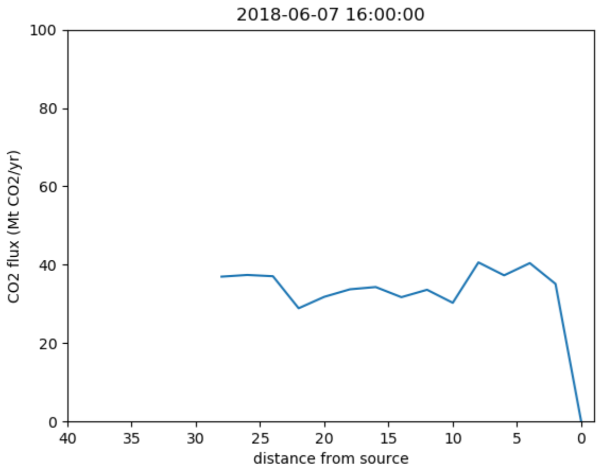

Figure 34: Estimation of fluxes as in Figure 33, but with wind speed in the direction of the plume taken from LES rather than being fixed.

The obtained results show little dependence on the width of the rectangles or on the size of the slabs over which the values are averaged (not shown). The values for the different rectangles show a variability of about 25% (e.g. Figure 33b) resulting mostly from assumptions made on wind direction and speed, and also the non-Gaussian nature of the plume which leads to the presence of pockets/puffs with elevated CO_2.

Current satellite missions targeting CO_2 with their swath of several kilometres cannot provide a complete image of the CO_2 plume. In case the plume direction is perpendicular to such narrow satellite path, the flux estimates can be calculated only over a few of the rectangles, thus reducing the robustness of the mean. For satellite path along the plume direction, centred on the source, only a part of the plume will be sampled leading to potentially reduced flux estimates as shown in Figure 35 (total resulting flux of 25.8 MtonCO$_2$/yr). The estimates further down from the source are more impacted as only a part of the plume is sampled. For any other direction, the number of available line density estimates decreases considerably as illustrated in Figure 36.

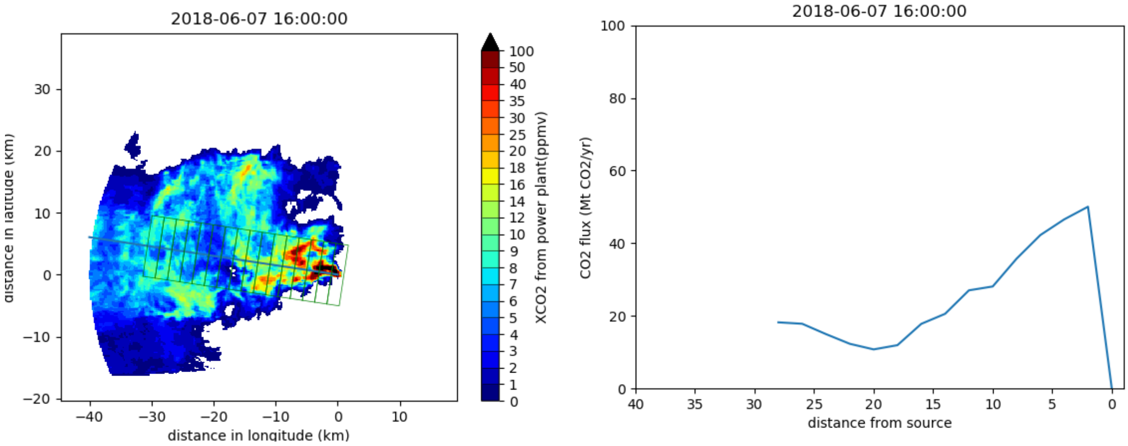

Figure 35: Estimation of fluxes as in Figure 33, but with swath width limited to 10 km.

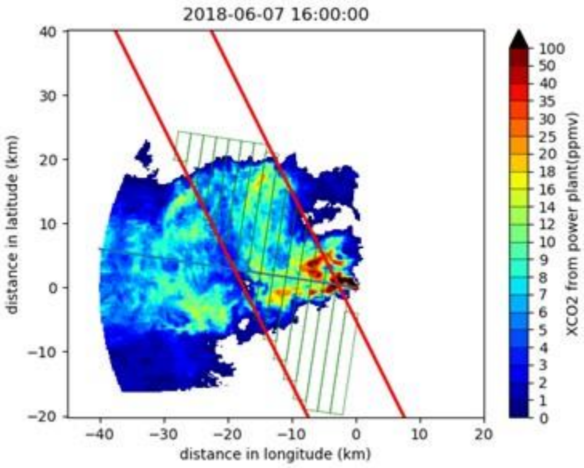

Figure 36: Illustration with satellite swath (indicated by red lines) inclined with respect to plume direction.

6 Conclusion

In an effort to support the top-down flux inversion methods, we have used the EULAG LES model to evaluate the spatio-temporal variability due to turbulence. Instruments based on polar orbiting satellites will be able to provide images of total CO_2 columns corresponding to a particular realisation of turbulent transport during the overpass. For days with high turbulent activity, the plume will likely contain intermittent and transient features (puffs) that might impact the flux inversion results. Considering this model uncertainty due to the transient nature of turbulent transport seems important.

In this study we have adapted the NCAR EULAG LES model (Wyszogrodzki et al., 2012) to simulate the transport of fossil fuel CO_2 from the Bełchatów power plant in Poland. The day chosen corresponds to the day for which CoMet data are available around the power plant. The observed data are used to evaluate the realism of the LES simulations. The EULAG model was adapted to be forced by the output from the mesoscale COSMO-GHG model at 1 km resolution. In general, the LES model is able to reproduce the measured wind speed and direction. However, during a significant part of the model simulation, the current setup leads to too stratified potential temperature profiles above 800 m thus limiting the uplifting of the plume above this altitude. For periods when the CO_2 was lifted to the upper part of the boundary layer, the characteristics of the simulated CO_2 plume features compare well with observations as far as plume width and spatio-temporal gradients are concerned.

Despite the described problem of generally too low altitude at which the model plume is transported, we have undertaken an analysis of spatio-temporal variability generated by the EULAG model. It is understood that the current limitations of the model setup might have an impact on the presented results. The current report is to be seen as resulting from work in progress that will be continued (see §7 with Perspectives).

The analysis of the LES simulated CO_2 fields from power plant emissions is indicating that both spatial and temporal variability within the plume are high for the selected day characterised by highly turbulent conditions. The variability decreases when the pixel size increases. However, even at low resolutions the simulated plume shows non-stationary features that distinguish it from a Gaussian plume.

The preliminary analysis of the impact of such features on two top-down flux retrieval methods was presented. For the methods based on OEM, it is proposed to include the model uncertainty due to the presence of turbulent like features in the inversion formalism. A very preliminary attempt to quantify this uncertainty at pixel level was proposed. This uncertainty was calculated for various pixel sizes, with values logically decreasing for larger pixels. Additional work on a more reliable quantification of XCO_2 model uncertainty for local scale transport of power plant plumes is needed. For the mass balance method, the impact of non-homogenous XCO_2 plumes on individual line densities at various distances from the source was demonstrated. In contrast to a Gaussian model for which the line densities are unchanged in time and as a function of distance from the source, strong variability was observed when LES output was used. The analysis needs to be consolidated as the current results rely on model transport close to the surface where the wind characteristics are different from those in the upper levels of the atmospheric boundary layer.

7 Perspectives

As a first step, the problem of increased vertical stability in the current setup of LES model will continue to be examined. The list of following ideas will be explored: longer spin-up time allowing more time for the PBL to build up, lowering the resolution to 100 m and 20 m in the horizontal and vertical directions respectively, and properly integrating the latent heat from COSMO-GHG that could provide the additional energy for modifying the model temperature profiles. Unfortunately, the deadline of this deliverable did not allow testing these solutions in time to be integrated in this report.

Once fully satisfactory results are obtained, the analysis of the variability on the flux retrieval methods will be repeated and further consolidated.

Work will be carried out on generating pseudo-observations from the LES model. Making the hypothesis that these pseudo-observations represent realistically the impact of variability due to turbulence, they will be used in flux OEM inversion studies under various hypothesis concerning the model transport and various versions of direct model transport (e.g. Gaussian hypothesis, CHIMERE).

Finally, a more systematic comparison of LES and COSMO-GHG transport will be carried out. One-to-one comparisons are not possible, and other quantitative indicators will be provided such as vertical distribution of the emitted CO_2, size of the puffs, spatio-temporal variability, etc. The indicators will be evaluated against CoMet observations.

It is proposed that the work outlined above is continued in the remaining months of the CHE project and also in the follow up projects that will hopefully follow.

8 Acknowledgments

We would like to thank Andrzej Wyszogrodzki of the Polish Meteorological Service for the help with the EULAG model.

We also thank the CoMet team for making the observation data available to this study.

9 References

Brunner, D., Kuhlmann, G., Marshall, J., Clément, V., Fuhrer, O., Broquet, G., Löscher, A., and Meijer, Y.: Accounting for the vertical distribution of emissions in atmospheric CO2 simulations, Atmos. Chem. Phys., 19, 4541–4559, https://doi.org/10.5194/acp-19-4541-2019, 2019.

Ciais, P., Crisp, D., Van Der Gon, H. D., Engelen, R., Heimann, M., Janssens-Maenhout, G., M. Heimann, Scholze, M. (2015). Towards a European operational observing system to monitor fossil CO_2 emissions, European Commission, Brussels, October 2015.

Crisp, David & Pollock, Randy & Rosenberg, Robert & Chapsky, Lars & Lee, Richard & Oyafuso, Fabiano & Frankenberg, Christian & O'Dell, Christopher & Bruegge, Carol & Doran, Gary & Eldering, Annmarie & Fisher, Bonnie & Fu, D. & Gunson, Michael & Mandrake, Lukas & Osterman, Gregory & Schwandner, Florian & Sun, Kang & Taylor, Tommy & Wunch, Debra. (2016). The On-Orbit Performance of the Orbiting Carbon Observatory-2 (OCO-2) Instrument and its Radiometrically Calibrated Products. Atmospheric Measurement Techniques Discussions. 1-45. 10.5194/amt-2016-281.

Krings, T., Gerilowski, K., Buchwitz, M., Reuter, M., Tretner, A., Erzinger, J., Heinze, D., Pflüger, U., Burrows, J. P., and Bovensmann, H.: MAMAP – a new spectrometer system for column-averaged methane and carbon dioxide observations from aircraft: retrieval algorithm and first inversions for point source emission rates, Atmos. Meas. Tech., 4, 1735–1758, https://doi.org/10.5194/amt-4-1735-2011, 2011.

Kuhlmann, G., Broquet, G., Marshall, J., Clément, V., Löscher, A., Meijer, Y., and Brunner, D.: Detectability of CO_2 emission plumes of cities and power plants with the Copernicus Anthropogenic CO_2 Monitoring (CO2M) mission, Atmos. Meas. Tech., 12, 6695–6719, https://doi.org/10.5194/amt-12-6695-2019, 2019.

Nassar, Ray & Hill, Timothy & Mclinden, Chris & Wunch, Debra & Jones, Dylan & Crisp, David. (2017). Quantifying CO_2 emissions from individual power plants from space. Geophysical Research Letters. 44. 10.1002/2017gl074702.

Prusa, Joseph & Smolarkiewicz, Piotr & Wyszogrodzki, Andrzej. (2008). EULAG, a Computational Model for Multiscale Flows. Computers & Fluids. 37. 1193-1207. 10.1016/j.compfluid.2007.12.001.

Takashi Hamazaki, "Greenhouse gases observation from space: overview of TANSO and GOSAT," Proc. SPIE 10566, International Conference on Space Optics — ICSO 2008, 1056621 (21 November 2017); https://doi.org/10.1117/12.2308255

Wyszogrodzki, Andrzej & Miao, Shiguang. (2012). Evaluation of the coupling between mesoscale-WRF and LES-EULAG models for the fine-scale urban dispersion. Atmospheric Research. 118. 324–345. 10.1016/j.atmosres.2012.07.023.

Document History

Version	Author(s)	Date	Changes
v0.1	Andrzej KLONECKI (SPASCIA)	29/09/2020	NA

Internal Review History

Internal Reviewers	Date	Comments
A.T.J. de Laat (KNMI)	18/10/2020	Approved with comments

Estimated Effort Contribution per Partner

Partner	Effort
SPASCIA	2PM
Total	**2PM**